2018

The pharmacokinetic model of 18F-FDOPA in PET brain imaging for early Parkinsonฺs disease

Wirunpatch Buratachwatanasiri
Faculty of Medicine

The pharmacokinetic model of ^{18}F-FDOPA in PET brain imaging for early Parkinson's disease

Miss Wirunpatch Buratachwatanasiri

A Thesis Submitted in Partial Fulfillment of the Requirements

for the Degree of Master of Science in Medical Imaging

Department of Radiology

Faculty of Medicine

Chulalongkorn University

Academic Year 2018

แบบจำลองทางเภสัชจลนศาสตร์ของ ^{18}F-FDOPA ในภาพเพทของสมองสำหรับผู้ป่วยโรคพาร์กินสันระยะแรกเริ่ม

น.ส.วิรัลพัชร บุรธัชวัฒนสิริ

วิทยานิพนธ์นี้เป็นส่วนหนึ่งของการศึกษาตามหลักสูตรปริญญาวิทยาศาสตรมหาบัณฑิต
สาขาวิชาฉายาเวชศาสตร์ ภาควิชารังสีวิทยา
คณะแพทยศาสตร์ จุฬาลงกรณ์มหาวิทยาลัย
ปีการศึกษา 2561

Thesis Title	The pharmacokinetic model of ^{18}F-FDOPA in PET brain imaging for early Parkinson's disease
By	Miss Wirunpatch Buratachwatanasiri
Field of Study	Medical Imaging
Thesis Advisor	Assistant Professor KITIWAT KHAMWAN, Ph.D.

Accepted by the Faculty of Medicine, Chulalongkorn University in Partial Fulfillment of the Requirement for the Master of Science

..... Dean of the Faculty of Medicine

(Professor SUTTIPONG WACHARASINDHU, M.D.)

THESIS COMMITTEE

..... Chairman

(Associate Professor SUPATPORN TEPMONGKOL, M.D.)

..... Thesis Advisor

(Assistant Professor KITIWAT KHAMWAN, Ph.D.)

..... Examiner

(Maythinee Chantadisai, M.D.)

..... External Examiner

(Franco Milano, Ph.D.)

วิรัลพัชร บุรธัชวัฒนสิริ : แบบจำลองทางเภสัชจลนศาสตร์ของ ^{18}F-FDOPA ในภาพเพทของสมองสำหรับผู้ป่วยโรคพาร์กินสันระยะแรกเริ่ม. (The pharmacokinetic model of ^{18}F-FDOPA in PET brain imaging for early Parkinson's disease) อ.ที่ปรึกษาหลัก : ผศ. ดร.กิติวัฒน์ คำวัน

โรคพาร์กินสันมักปรากฏอาการเมื่อจำนวนเซลล์ที่ผลิตโดปามีนสูญเสียไปมากกว่าครึ่งหนึ่ง เพราะฉะนั้นการวินิจฉัยและรักษาโรคในระยะแรกเริ่มจึงมีสำคัญอย่างยิ่ง การตรวจเพท ^{18}F-FDOPA ถูกใช้อย่างแพร่หลายเพื่อคัดแยกความผิดปกติในกระบวนการเมตาบอลิสมของสารโดปามีนในสมองมนุษย์ วัตถุประสงค์ของการศึกษาวิจัยนี้เพื่อหาค่าคงที่อัตราการแลกเปลี่ยนสาร ^{18}F-FDOPA จากภาพเพทของสมองผู้ป่วยโรคพาร์กินสันระยะแรกเริ่มโดยอาศัยแบบจำลองทางเภสัชจลนศาสตร์ งานวิจัยนี้ทำการศึกษาโดยใช้ข้อมูลย้อนหลังของผู้ป่วยโรคพาร์กินสันระยะแรกเริ่มจำนวน 5 รายที่ทำการตรวจภาพสมองด้วยเครื่องเพทซีที ณ โรงพยาบาลจุฬาลงกรณ์ สภากาชาดไทย การเก็บข้อมูลภาพเพททำทันทีหลังจากฉีดสาร ^{18}F-FDOPA โดยใช้เวลาเก็บข้อมูล 90 นาทีด้วย list-mode 3 มิติ และสร้างภาพที่มีระยะห่างของช่วงเวลาทุก 5 นาทีเพื่อให้ได้ชุดข้อมูลภาพในแต่ละช่วงเวลา จากนั้นนำไปลงทะเบียนภาพและปรับภาพให้เท่ากับภาพเพทแม่แบบของสมองด้วยโปรแกรม Statistical Parametric Mapping (SPM) เพื่อทำการแบ่งส่วนภาพบริเวณ striatum, caudate และ putamen แล้ววัดค่าความเข้มข้นรังสีในแต่ละข้างของบริเวณดังกล่าว แบบจำลองทางเภสัชจลนศาสตร์และ Time-activity curve ถูกสร้างด้วยโปรแกรมซิมูเลชั่น SAAM II เพื่อคำนวณหาค่าอัตราคงที่แลกเปลี่ยนสารในแต่ละข้างของส่วนสมอง โดยข้างที่อยู่ตรงข้ามกับอาการเด่นของคนไข้จะถูกพิจารณาเป็นตัวแทนของโรคพาร์กินสัน ส่วนอีกข้างถูกพิจารณาให้เป็นตัวแทนในคนปกติ แบบจำลองที่พัฒนาขึ้นประกอบด้วย 3 ส่วนแบ่ง และ 3 อัตราคงที่แลกเปลี่ยนสารซึ่งเพียงพอต่อการคำนวณชีวจลนศาสตร์ของ ^{18}F-FDOPA และเมตาโบไลท์ ผลการวิจัยพบว่าอัตราคงที่แลกเปลี่ยนสารเข้าและออกข้ามตัวกรองกั้นระหว่างเลือดและสมอง (K_1 และ k_2) และอัตราคงที่ปฏิกิริยาดีคาร์บอกซิเลชั่น (k_3) ในบริเวณ striatum ข้างที่เป็นโรค มีค่าเฉลี่ยเท่ากับ 0.0231 ± 0.0081 ml min^{-1} g^{-1}, 0.0196 ± 0.0054 min^{-1}, และ 0.0112 ± 0.0043 min^{-1} ตามลำดับ ส่วนข้างที่ปกติ มีค่าเฉลี่ยเท่ากับ 0.0245 ± 0.0078 ml min^{-1} g^{-1}, 0.0178 ± 0.0061 min^{-1} และ 0.0152 ± 0.0053 min^{-1} ตามลำดับ สำหรับส่วน caudate ข้างที่เป็นโรค K_1 = 0.0094 ± 0.0030 ml min^{-1} g^{-1}, k_2 = 0.0237 ± 0.007 min^{-1}, และ k_3 = 0.0203 ± 0.0077 min^{-1} ส่วนข้างที่ไม่เป็นโรค K_1 = 0.0091 ± 0.0022 ml min^{-1} g^{-1}, k_2 = 0.0228 ± 0.0031 ± 0.0057 min^{-1} และ k_3 = 0.0215 ± 0.0094 min^{-1} ใน putamen ข้างที่เป็นโรค K_1 = 0.0116 ± 0.0037 ml min^{-1} g^{-1}, k_2 = 0.0268 min^{-1} และ k_3 = 0.0112 ± 0.003 min^{-1} ในขณะที่ข้างปกติ K_1 = 0.0131 ± 0.0044 ml min^{-1} g^{-1}, k_2 = 0.0254 ± 0.0072 min^{-1} และ k_3 = 0.0176 ± 0.0025 min^{-1} นอกจากนี้ยังพบว่าสมองส่วน striatum และ putamen ในข้างที่มีความผิดปกติจะมีค่า K_1 และ k_3 น้อยกว่าข้างที่ปกติอย่างมีนัยสำคัญทางสถิติ (p-value < 0.05) ในทางกลับกันพบว่าไม่มีความแตกต่างของค่าอัตราคงที่แลกเปลี่ยนสารในสมองส่วน caudate ซึ่งข้อมูลชีวจลนศาสตร์ที่ได้จากการศึกษาวิจัยครั้งนี้คาดว่าจะถูกใช้เป็นค่าอ้างอิงเริ่มต้นในคนไข้โรคพาร์กินสันในประเทศไทยในอนาคต โดยค่าคงที่อัตราการแลกเปลี่ยนสาร K_1 และ k_3 อาจใช้เป็นตัวคัดแยกความแตกต่างระหว่างคนไข้โรคพาร์กินสันและคนปกติได้

สาขาวิชา	ฉายาเวชศาสตร์	ลายมือชื่อนิสิต .....
ปีการศึกษา	2561	ลายมือชื่อ อ.ที่ปรึกษาหลัก .....

6074092630 : MAJOR MEDICAL IMAGING

KEYWORD: PET/CT, 18F-FDOPA, Parkinson's disease, compartmental model, Statistical Parametric Mapping

Wirunpatch Buratachwatanasiri : The pharmacokinetic model of ^{18}F-FDOPA in PET brain imaging for early Parkinson's disease. Advisor: Asst. Prof. KITIWAT KHAMWAN, Ph.D.

Parkinson's disease (PD) symptom usually appears when over half of all dopaminergic neurons have died. Early detection and treatment approach are; therefore, very important. The ^{18}F-FDOPA PET scan is extensively examined to differentiate the normal and pathological dopamine metabolism in the human brain. The purpose of this study was to investigate the transfer rate constants of ^{18}F-FDOPA in PET brain imaging based on compartmental model in early Parkinson's disease. The retrospective data from five early PD patients who underwent ^{18}F-FDOPA PET brain scan at King Chulalongkorn Memorial Hospital (KCMH) were collected. After ^{18}F-FDOPA was administered intravenously, PET images were acquired for 90 min using 3D list-mode and reconstructed into 5-min interval for obtaining each time-point image dataset. PET image data were co-registered and normalized with PET brain template on Statistical Parametric Mapping (SPM) software for segmenting the striatum, caudate and putamen. The activity concentration was subsequently measured at each side of the regions. Compartmental model and time-activity curve were generated using SAAM II simulation software to estimate transfer rate constants in each side. Regions at contralateral side to patient's predominant symptoms were considered as PD and the ipsilateral side as control. A pharmacokinetic model consisting of 3 compartments and 3 transfer rate constants could adequately describe the kinetics ^{18}F-FDOPA and its metabolites. By model fitting to the tissue kinetics, the mean FDOPA forward and reverse transport constant across the blood-brain barrier (K_1 & k_2), and the mean FDOPA decarboxylation rate constant (k_3) in the contralateral striatum were $K_1 = 0.0231 \pm 0.0081$ ml min^{-1} g^{-1}, $k_2 = 0.0196 \pm 0.0054$ min^{-1}, and $k_3 = 0.0112 \pm 0.0043$ min^{-1} while the ipsilateral striatum were $K_1 = 0.0245 \pm 0.0078$ ml min^{-1} g^{-1}, $k_2 = 0.0178 \pm 0.0061$ min^{-1}, and $k_3 = 0.0152 \pm 0.0053$ min^{-1} respectively. For the contralateral caudate, $K_1 = 0.0094 \pm 0.0030$ ml min^{-1} g^{-1}; $k_2 = 0.0237 \pm 0.007$ min^{-1}; and $k_3 = 0.0203 \pm 0.0077$ min^{-1} while the ipsilateral, $K_1 = 0.0091 \pm 0.0022$ ml min^{-1} g^{-1}; $k_2 = 0.0228 \pm 0.0031$ min^{-1}; and $k_3 = 0.0215 \pm 0.0094$ min^{-1}. In the contralateral putamen, $K_1 = 0.0116 \pm 0.0037$ ml min^{-1} g^{-1}; $k_2 = 0.0268 \pm 0.0057$ min^{-1}; and $k_3 = 0.0112 \pm 0.003$ min^{-1}, while the ipsilateral, $K_1 = 0.0131 \pm 0.0044$ ml min^{-1} g^{-1}; $k_2 = 0.0254 \pm 0.0072$ min^{-1}; and $k_3 = 0.0176 \pm 0.0025$ min^{-1}. Furthermore, K_1 and k_3 rate constants at the contralateral side of striatum and putamen were significantly lower than the another (p-value < 0.05). In contrast, there was no statistically significant difference in any transfer rate constants of caudate. The biokinetic data obtained in this study will be used as an initial reference report in Thai PD patients. Both K_1 and k_3 seemed to be the predictor parameters to distinguish between PD and normal patients.

Field of Study:	Medical Imaging	Student's Signature .....
Academic Year:	2018	Advisor's Signature .....

ACKNOWLEDGEMENTS

The success of this thesis depends on the contribution of many people. First of all, I wish to express gratitude and deepest appreciation Assistant Professor Dr. Kitiwat Khamwan for his helpful, supervision, guidance, encouragement and invaluable advice during the whole study.

I wish to express gratitude and appreciation to Miss Maythinee Chantadisai, M.D., my co-advisor for her help in the clinical knowledge, assistance and suggestion for this work.

I would like to greatly thank Assistant Professor Dr. Yothin Rakvongthai and Miss Jaruwan Onwanna for their help in Statistical Parametric Mapping (SPM) program.

I wish to express the deepest appreciation to Associate Professor Dr.Anchali Krisanachinda, Associate Professor Sivalee Suriyapee and Professor Franco Milano for their valuable suggestion to this study.

I gratefully acknowledge the member of my thesis committee: Associate Professor Supatporn Tepmongkol, M.D. for their valuable suggestion and guidance.

I would like to thank nuclear medicine technologists, medical physicists, nuclear medicine physicians and staffs at Division of Nuclear Medicine, King Chulalongkorn Memorial Hospital for their kind contribution and suggestion to this work.

I also wish to express gratitude to all lecturers and staff in the Master of Science Program in Medical Imaging, Department of Radiology, Faculty of Medicine, Chulalongkorn University for their unlimited teaching throughout whole study.

Last but not least, my gratefulness to every member in my family for their financial supports, valuable encouragement and entirely cares during the course study.

Wirunpatch Buratachwatanasiri

TABLE OF CONTENTS

Page

ABSTRACT (THAI) iii

ABSTRACT (ENGLISH) iv

ACKNOWLEDGEMENTS v

TABLE OF CONTENTS vi

LIST OF TABLES ix

LIST OF FIGURES x

LIST OF ABBREVIATIONS xiii

CHAPTER 1 INTRODUCTION 1

1.1 Background and Rationale 1

1.2 Research Objective 2

1.3 Definitions 2

CHAPTER 2 REVIEW OF RELATED LITERATURE 4

2.1 Theory 4

2.1.1 Parkinson's Disease 4

2.1.1.1 Pathophysiology 4

2.1.1.2 Clinical Signs and Symptoms 6

2.1.1.3 Hoehn and Yahr Scale (HY) 6

2.1.1.4 Diagnostic 7

2.1.2 Positron Emission Tomography (PET) 8

2.1.2.1 Basic Principles 8

2.1.2.2 PET Image Formation 9

2.1.2.3 Data Acquisition 9

2.1.3 6-[^{18}F]Fluoro-L-DOPA (^{18}F-FDOPA).....10

2.1.4 ^{18}F-FDOPA PET Neuroimaging in PD 11

2.1.5 Kinetic Modeling in Positron Emission Tomography 12

2.1.6 Akaike's Information Criterion (AIC).....13

2.1.7 Bayesian Information Criterion (BIC) 14

2.2 Review of Related Literatures.....15

CHAPTER 3 RESEARCH METHODOLOGY 17

3.1 Research Design.....17

3.2 Research Design Model 17

3.3 Conceptual Framework 18

3.4 Research Question.....18

3.5 Key Words.....18

3.6 The Sample.....18

3.6.1 Target Population.....18

3.6.2 Sample Population 18

3.6.3 Eligible Criteria.....19

3.6.3.1 Inclusion Criteria 19

3.6.3.2 Exclusion Criteria 19

3.6.4 Sample Size Determination.....19

3.7 Materials.....20

3.7.1 Positron Emission Tomography/Computed Tomography (PET/CT) 20

3.7.2 Statistical Parametric Mapping (SPM) 20

3.7.3 Image J 21

3.7.4 SAAM II 22
3.8 Methods 23
3.8.1 PET/CT System Quality Control 23
3.8.2 Patients Data Collection 23
3.8.3 Automated Image Segmentation Using SPM 24
3.8.4 Activity Concentration Measurement 29
3.8.5 ^{18}F-FDOPA Pharmacokinetic Modeling for PD Patients 30
3.9 Statistical Analysis 32
3.10 Ethical Consideration 32
3.11 Expected Benefits 32
CHAPTER 4 RESULTS 33
4.1 Quality Control of PET/CT System 33
4.2 Biodistribution Data of ^{18}F-FDOPA 33
4.3 Biokinetic Data of ^{18}F-FDOPA 46
CHAPTER 5 DISCUSSION AND CONCLUSIONS 59
5.1 Discussion 59
5.2 Conclusions 64
REFERENCES 65
APPENDICES 68
APPENDIX A Report of PET/CT System Quality Control 69
APPENDIX B The Approval of Institutional Review Board 73
APPENDIX C Case Record Form 74
VITA 84

LIST OF TABLES

Page

Table 1 Hoehn and Yahr Scale. 6

Table 2 The expression of each template. 26

Table 3 The clinical characteristics of five patients' data. 33

Table 4 Percentage of injected activity in contralateral striatum. 37

Table 5 Percentage of injected activity in ipsilateral striatum. 38

Table 6 Percentage of injected activity in contralateral caudate. 39

Table 7 Percentage of injected activity in ipsilateral caudate. 40

Table 8 Percentage of injected activity in contralateral putamen. 41

Table 9 Percentage of injected activity in ipsilateral putamen. 42

Table 10 Transfer rates of striatum. 54

Table 11 Transfer rates of caudate. 55

Table 12 Transfer rates of putamen. 56

Table 13 AIC and BIC of the model in each region. 58

Table 14 The comparison of transfer rate constant between literatures review and this study. 61

Table 15 Percent contrast and lung residual error with source-to-background ratio 4:1. 71

Table 16 Percent contrast and lung residual error with source-to-background ratio 8:1. 72

LIST OF FIGURES

Page

Figure 1 The sites of neurodegeneration and neurochemical pathways involved in Parkinson's disease[5]. 5

Figure 2 Positron emission and annihilation[8]. 8

Figure 3 Schematic diagram illustrating the various transport and biochemical pathways of FDOPA in the human body. 10

Figure 4 Transverse ^{18}F-FDOPA PET images of a healthy control (Left) and a patient with idiopathic PD (Right)[13]. 11

Figure 5 One-tissue compartment model[17]. 13

Figure 6 Compartmental model describing for the ^{18}F-FDOPA kinetics in Huang's study. 15

Figure 7 Compartmental model describing for the ^{18}F-FDOPA kinetics according to Kuwabara's study. 16

Figure 8 Compartmental model describing for the ^{18}F-FDOPA kinetics according to Wahl and Nahmias's study. 16

Figure 9 Research design model. 17

Figure 10 Conceptual framework. 18

Figure 11 PET/CT system model Siemens Biograph16. 20

Figure 12 Statistical Parametric Mapping (SPM) software. 21

Figure 13 ImageJ. 21

Figure 14 SAAM II. 22

Figure 15 Positioning of IEC body phantom for testing image quality of PET/CT system. 23

Figure 16 A series of PET images reconstructed with 5-min interval from 0 to 85-minute time points. 24

Figure 17 (A) MRI referenced image, and (B) PET reoriented images. 24

Figure 18 (A) the histograms for the images in the original orientations, and the final orientations, (B) the PET reference image, and (C) PET registered images. 25

Figure 19 (A) The PET template, and (B) The normalized patient image. 26

Figure 20 The superimposing of normalized patient images and striatum template (cyan color) in coronal, sagittal, and transverse planes. (Right lower) The final result image of striatum segmentations using the SPM. 27

Figure 21 The segmented striatum (A), caudate (B) and putamen (C) in every time points. 28

Figure 22 (Left) The original image, and (Right) The normalized image. 29

Figure 23 (A) ROI over one side of the segmented striatum, and (B) the histogram. 29

Figure 24 PET ^{18}F-FDOPA brain scan, (arrow) lower uptake at left putamen. 30

Figure 25 Compartmental model describing the kinetics of ^{18}F-FDOPA for PD patients in SAAM II. 31

Figure 26 Percent injected activities were input into SAAM II. 31

Figure 27 Patient 1's PET ^{18}F-FDOPA brain images in each time point. 34

Figure 28 Patient 2's PET ^{18}F-FDOPA brain images in each time point. 34

Figure 29 Patient 3's PET ^{18}F-FDOPA brain images in each time point. 35

Figure 30 Patient 4's PET ^{18}F-FDOPA brain images in each time point. 35

Figure 31 Patient 5's PET ^{18}F-FDOPA brain images in each time point. 36

Figure 32 Box plots of percentage of injected activity in contralateral (upper) and ipsilateral (lower) striatum in each time point. 43

Figure 33 Box plots of percentage of injected activity in contralateral (upper) and ipsilateral (lower) caudate in each time point. 44

Figure 34 Box plots of percentage of injected activity in contralateral (upper) and ipsilateral (lower) putamen in each time point. 45

Figure 35 The Patient no 1's time-activity curves in the striatum (A), caudate (B) and putamen (C). 47

Figure 36 The Patient no 2's time-activity curves in the striatum (A), caudate (B) and putamen (C). 48

Figure 37 The Patient no 3's time-activity curves in the striatum (A), caudate (B) and putamen (C). 49

Figure 38 The Patient no 4's time-activity curves in the striatum (A), caudate (B) and putamen (C). 50

Figure 39 The Patient no 5's time-activity curves in the striatum (A), caudate (B) and putamen (C). 51

Figure 40 The mean time-activity curves in the striatum (A), caudate (B) and putamen (C). 53

Figure 41 Box plots of transfer rate constants in contralateral (red) and ipsilateral (blue) striatum. 56

Figure 42 Box plots of transfer rate constants in contralateral (red) and ipsilateral (blue) caudate. 57

Figure 43 Box plots of transfer rate constants in contralateral (red) and ipsilateral (blue) putamen. 57

Figure 44 Box plots of transfer rate constants in ipsilateral striatum (normal) compared between literatures review and this study.....62

Figure 45 Box plots of transfer rate constants in contralateral striatum (PD) compared between literatures review and this study.....62

Figure 46 Positioning of IEC body phantom and scatter phantom for testing image quality of PET/CT system. 70

Figure 47 Example of ROIs placement on IEC body phantom image for quantitative analysis. ..70

Figure 48 Percent contrast with source-to-background ratio 4:1 and 8:1. 72

LIST OF ABBREVIATIONS

^{18}F-FDOPA	L-3,4-Dihydroxy-6-[^{18}F]fluorophenylalanine
3-OMFD	3-O-methyl-6-[^{18}F]fluoro-L-dopa
AAAD	Aromatic L-Amino Acid Decarboxylase
AAL	Automated Anatomical Labeling
AIC	Akaike Information Criterion
BBB	Blood Brain Barrier
BIC	Bayes Information Criterion
CFOV	Center of Field of View
COMT	Catechol-O-Methyltransferase
DDC	DOPA Decarboxylase
FDA	[^{18}F]fluorodopamine
FDOPAC	[^{18}F]6-fluoro-3,4-dihydroxyphenylacetic acid
FHVA	[^{18}F]6-fluorochomovanillic acid
FOV	Field of View
FWHM	Full-Width at Half Maximum
GPi	Globus Pallidus Interna
HY scale	Hoehn and Yahr scale
ICBM	International Consortium for Brain Mapping
IEC	International Electric Commission
KCMH	King Chulalongkorn Memorial Hospital
L-DOPA	Dihydroxyphenylalanine
MRI	Magnetic Resonance Imaging
PD	Parkinson's Disease
PET	Positron Emission Tomography
ROI	Region of Interest
TAC	Time-Activity Curve
VOI	Volume of Interest

CHAPTER 1

INTRODUCTION

1.1 Background and Rationale

Parkinson's disease is the second most common neurodegenerative disorder, caused by the progressive impairment of dopaminergic neurons in the basal ganglia and deterioration of neurons in substantia nigra. Normally, these neurons produce neurotransmitter known as dopamine, which is a chemical messenger that allows communication between the substantia nigra and corpus striatum. As a result, this communication coordinates smooth and balanced muscle movement. When over half of dopaminergic neurons is lost, it affects the effective control of movements[(1)].

Presently, the clinical diagnosis of PD relies on the presence of cardinal motor features include rigidity, bradykinesia and resting tremors, losses of dopamine in the striatum and a favorable response to dopaminergic therapy. However, the diagnosis of PD can be difficult because several neurodegenerative disorders such as progressive supranuclear palsy, multi-system atrophy, cortico basal degeneration, and vascular parkinsonism may present with similar signs and symptoms. Furthermore, it is more difficult to diagnose PD in its early stage because of signs may be mild and go unnoticed. Therefore, the clinical diagnosis alone is not accurate enough and this reinforces the importance of the functional imaging aiming at the detection of pathophysiology of the disease process.

Over the past decade, in-vivo imaging of the nigrostriatal dopaminergic system has provided an opportunity to use objective methods to measure the severity and progression of PD. Dopaminergic dysfunction in patients with PD has been visualized with positron emission tomography (PET) which is a powerful nuclear medicine imaging technique enabling the estimation of important physiological parameters. PET, especially with L-3,4-Dihydroxy-6-[^{18}F] fluorophenylalanine (^{18}F-FDOPA) as the tracer, has been used to demonstrate and to quantify presynaptic dopaminergic function. The uptake of ^{18}F-FDOPA PET expresses the activity of the dopa-decarboxylase enzyme in the striatal nerve terminals of dopamine neurons, correlates with dopamine storage capacity.

Interpretation of ^{18}F-FDOPA PET imaging is mostly performed by qualitative examination of the relative radioactivity distribution in the striatum. The unilaterally decreased ^{18}F-FDOPA uptake on the contralateral side to patient's symptom has been reported in the striatum in early PD patient. The depletion is more severe in the putamen than in the caudate nucleus and is most prominent in the caudal parts of the putamen because of the topographic organization of the nigrostriatal projection. However, ^{18}F-FDOPA PET brain should yield the quantitative measurement of ^{18}F-FDOPA which represent the biokinetic and may reliably discriminate between patient and normal subjects for highest clinical usefulness[(2)].

Compartmental model is one of most widely approaches for PET quantitative analysis, assume that the brain is composed by a number of interacting subsystems called compartments, and exchange material with other compartments. By acquiring dynamic PET images, it is possible to obtain the distribution of the radiotracer over time at different brain substructures and transform regional tissue radioactivity into the rate of a physiological or biochemical process. This can be determined using a mathematical model to describe the kinetics of tracer uptake in relation to the rate of the process of interest.

1.2 Research Objective

To investigate the transfer rate constants of ^{18}F-FDOPA in PET brain imaging based on compartmental model in patient with early Parkinson's disease.

1.3 Definitions

Akaike information criterion (AIC)	An estimator of the relative quality of statistical models for a given set of data.
Bayes information criterion	A criterion for model selection among a finite set of models.
Carbidopa	A drug given to people with Parkinson's disease in order to inhibit peripheral metabolism of levodopa.
Compartment	A physical location where a substance resides or a specific chemical state of the substance under study.
Contralateral side	The opposite of predominant symptoms which had lower uptake in striatum, caudate or putamen.
^{18}F-FDOPA (L-3,4-Dihydroxy-6-[^{18}F] fluorophenylalanine)	A PET radiopharmaceutical which analog to L-DOPA, the immediate precursor of dopamine.
Ipsilateral side	The side of predominant symptoms which had normal uptake in striatum, caudate or putamen.

K_1	The forward transport rate constants of plasma FDOPA across the blood brain barrier to the tissue FDOPA compartment.
k_2	The reverse transport rate constants of plasma FDOPA across the blood brain barrier to the tissue FDOPA compartment.
k_3	The FDOPA decarboxylation rate constant from the tissue FDOPA compartment to the combined compartment of FDA and its metabolites.
Parkinson's disease	A progressive nervous system disorder that affects movement.
Pharmacokinetic model	A mathematical modeling technique for predicting the absorption, distribution, metabolism and excretion (ADME) of synthetic or natural chemical substances in humans and other animal species.
Positron Emission Tomography	A modality generates images depicting the distributions of positron-emitting nuclides in patients.
Transfer rate constant	The fractional rate of physiological or biochemical transfer process.

CHAPTER 2

REVIEW OF RELATED LITERATURE

2.1 Theory

2.1.1 Parkinson's Disease

Parkinson's disease is named after James Parkinson, an English physician who described it in his work entitled an assay on the shaking palsy from 1817. The disease is a progressive neurodegenerative disorder caused by the loss of dopaminergic nigrostriatal neurons. PD is a type of movement disorder that can affect the ability to perform common, daily activities. The most prominent clinical features include resting tremor, rigidity, bradykinesia and postural instability. Although there are common symptoms of PD, they can vary greatly from person to person. Moreover, how these symptoms change over time and whether other symptoms of PD emerge differ from person to person. Most people who develop the symptoms of PD do so sometime after the age of 50, but PD can affect younger persons as well[3].

2.1.1.1 Pathophysiology

Parkinson's disease is characterized by the progressive death of selected but heterogeneous populations of neurons (Figure 1), including the neuromelanin-laden dopaminergic neurons of the pars compacta of the substantia nigra, selected aminergic brain-stem nuclei (both catecholaminergic and serotoninergic), the cholinergic nucleus basalis of Meynert, hypothalamic neurons, and small cortical neurons (particularly in the cingulate gyrus and entorhinal cortex), as well as the olfactory bulb, sympathetic ganglia, and parasympathetic neurons in the gut. Not all dopaminergic projection areas are equally susceptible. Within the substantia nigra pars compacta, neuronal loss tends to be greatest in the ventrolateral tier (loss is estimated to be 60 to 70 percent at the onset of symptoms), followed by the medial ventral tier and dorsal tier. This pattern of cell loss is relatively specific to Parkinson's disease; it is the opposite of that seen in normal aging and differs from patterns found in striatonigral degeneration and progressive supranuclear palsy. It results in a regional loss of striatal dopamine, most prominently in the dorsal and intermediate subdivisions of the putamen, a process that is believed to account for akinesia and rigidity. This pattern of cell loss also correlates with the degree of expression of messenger RNA for the dopamine transporter. Another important pathological feature is the presence of degenerating ubiquitin-positive neuronal processes or neurites (Lewy neurites), which are found in all affected brain-stem regions, especially the dorsal motor nucleus of the vagus[4].

It has been suggested that a greater degree of medial nigral cell loss, with enhanced involvement of projections to the caudate nucleus, could result in more cognitive dysfunction. Other potential factors in the varied cognitive changes in Parkinson's disease include the involvement of other subcortical structures, such as the nucleus basalis of Meynert and locus caeruleus, and cerebral cortical areas, especially the entorhinal cortex[5].

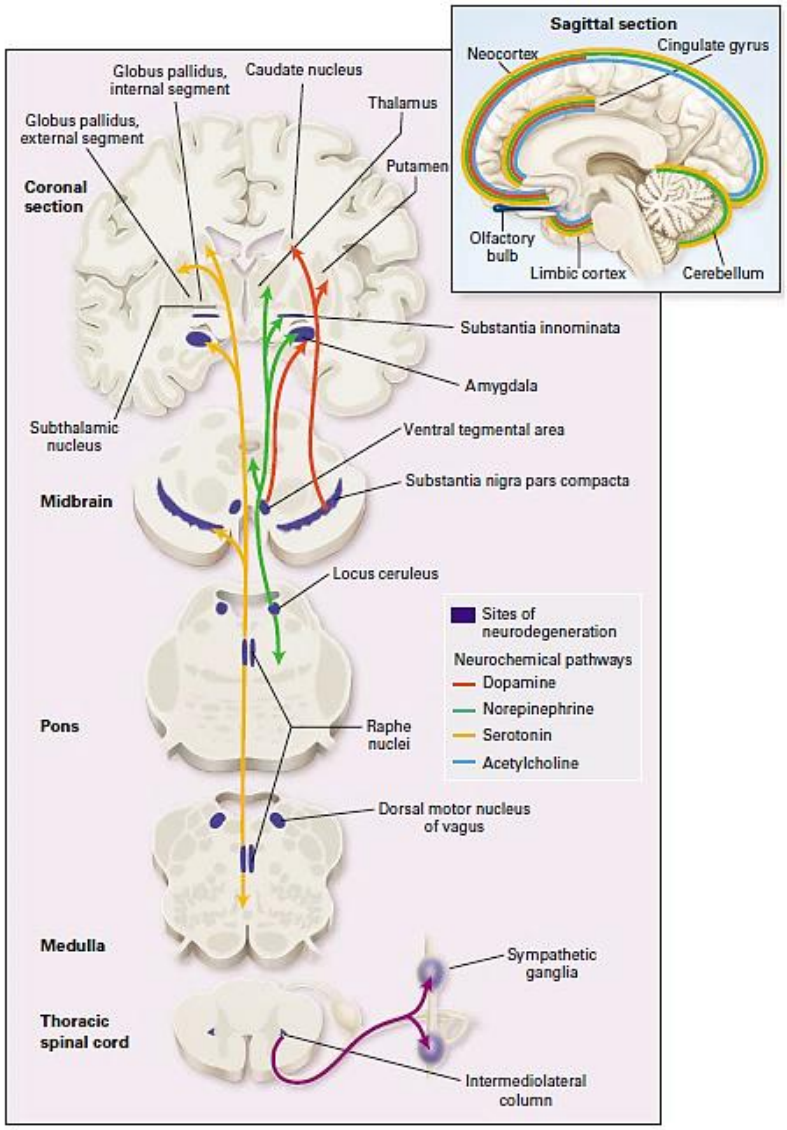

Figure 1 The sites of neurodegeneration and neurochemical pathways involved in Parkinson's disease[5].

2.1.1.2 Clinical Signs and Symptoms

There are five primary motor symptoms of PD: tremor, rigidity, bradykinesia (slow movement), postural instability (balance problems), and walking/gait problems. Observing one or more of these symptoms is the main way that physicians diagnose PD. However, symptoms of PD can vary greatly from individual to individual—both in terms of their intensity and how they progress[1].

2.1.1.3 Hoehn and Yahr Scale (HY)

The Hoehn and Yahr scale (HY) is a widely used clinical rating scale, which defines broad categories of motor function in Parkinson's disease. Among its advantages are that it is simple and easily applied. It captures typical patterns of progressive motor impairment which can be applied whether or not patients are receiving dopaminergic therapy. Progression in HY stages has been found to correlate with motor decline, deterioration in quality of life, and neuroimaging studies of dopaminergic loss. A modified version of HY is sometimes used[6].

Table 1 Hoehn and Yahr Scale.

Hoehn and Yahr Scale	**Modified Hoehn and Yahr Scale**
1: Only unilateral involvement, usually with minimal or no functional disability	1.0: Unilateral involvement only
	1.5: Unilateral and axial involvement
2: Bilateral or midline involvement without impairment of balance	2.0: Bilateral involvement without impairment of balance
3: Bilateral disease: mild to moderate disability with impaired postural reflexes; physically independent	2.5: Mild bilateral disease with recovery on pull test
	3.0: Mild to moderate bilateral disease; some postural instability; physically independent
4: Severely disabling disease; still able to walk or stand unassisted	4.0: Severe disability; still able to walk or stand unassisted
5: Confinement to bed or wheelchair unless aided	5.0: Wheelchair bound or bedridden unless aided

2.1.1.4 Diagnostic

PD is diagnosed by clinical criteria; there is no definitive test for the diagnosis. Historically, pathologic confirmation of the hallmark of Lewy body on autopsy has been considered the criterion standard for the diagnosis. Nowadays, the gold standard for the diagnosis of Parkinson's disease changes to the neuropathological examination. The diagnosis of Parkinson's disease is made on the basis of clinical criteria developed by the UK Parkinson's Disease Society Brain Bank. The classic triad of major signs of Parkinson's disease is made up of tremor, rigidity, and akinesia. Differentiating PD from other forms of parkinsonism can be challenging early in the course of the disease, when signs and symptoms overlap with other syndromes. Unfortunately, there is still no biologic marker that unequivocally confirms the diagnosis[4].

In addition to taking a history and performing a detailed neurologic examination, physicians sometimes use brain imaging to help support a particular diagnosis. Imaging studies to evaluate PD such as magnetic resonance imaging (MRI), which show the changes in anatomical structure of the brain[5]. Another diagnostic imaging study is DaTscan, an imaging test that measures dopamine function in the brain. Because other parkinsonian syndromes may also have abnormal dopamine function, DaTscan cannot reliably distinguish between PD and other parkinsonian syndromes, but may be particularly useful for the refinement of a diagnosis if a person with PD symptoms does not respond to the usual PD medications. Other imaging studies that can be done, include functional MRI (fMRI), a specialized form of brain imaging that examines brain function, and positron emission tomography (PET), which can measure certain brain functions[1].

2.1.2 Positron Emission Tomography (PET)

2.1.2.1 Basic Principles

A positron is an antiparticle of an electron with identical mass and charge. After emission, positron travels for a short distance from its site of origin, gradually losing energy through multiple collisions with electrons present in the neighboring tissues. When most of its kinetic energy has been lost, the positron reacts with a resident electron in an annihilation reaction. This reaction generates two gamma photons of 511 keV each (which is resting energy of the electron or positron in opposite direction as depicted in the Figure 2. This ensures conservation of energy and momentum. The unique characteristic of simultaneous emission of two annihilated photons forms the basis for detection and localization of positron emitters using a novel technique called coincidence detection[7].

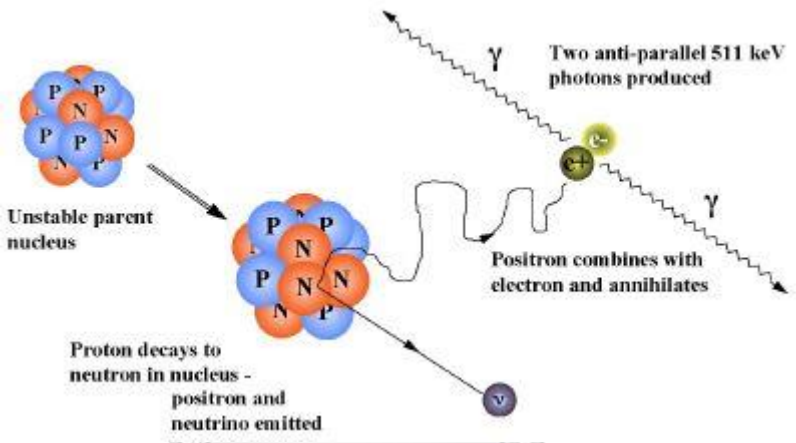

Figure 2 Positron emission and annihilation[8].

Scintillation detectors - e.g., bismuth germinate (BGO) or Lutetium Oxyorthosilicate (LSO) and photomultiplier tubes are placed opposite to the source of positron emitter. The signals are then fed into separate amplifiers and energy discriminating circuits. This process results into detection of a coincidence event, which localizes an annihilation event somewhere along the line joining the two detectors. In a typical PET scanner, there are hundreds of such points of detector banks in the form of ring surrounding the patient. It can, therefore, be stated that the PET scanning in a comprehensive manner relates to detection of millions of coincidence events, defines a line along which the annihilation reaction occurred and hence provides information about the concentration and spatial location of positron emitters within the patient.

2.1.2.2 PET Image Formation

Each pair of parallel and opposite detectors produces a coincidence line, which is unique in terms of location and direction. A large number of such coincidence lines form the data set and by the use of which a cross-sectional image can be reconstructed. The data pertaining to coincidence events is stored as two-dimensional matrix in which horizontal direction represents offset from the center of the field of view (CFOV), whereas vertical direction describes the projection angle. This set of data in terms of two-dimensional matrix is called 'Sinogram' and provides a set of projection data for reconstruction of image. Sinogram data however needs to be corrected for tissue alternations as well as detector non-uniformities. Various detector elements in a PET system are expected to exhibit variation in detection efficiency due to geometrical variation, differences in energy discrimination as well as detector gains. Such variations need to be equalized to prevent appearance of any artifacts. In addition, attenuation correction accounts for the compensation due to intra-tissue absorption of one or both annihilated photons. After necessary corrections, the Sinogram cumulatively represents all the coincidence events along a particular coincidence line. Sinogram data is then used to reconstruct the image using filtered back projection or an interactive technique[9].

2.1.2.3 Data Acquisition

The data acquisition can be applied to both static and dynamic imaging of an object using the frame mode of data collection. In static imaging, a frame is obtained consisting of a set of sinograms acquired over the length of the scan, whereas in dynamic imaging, the data are collected in multiple frames of sinograms, each of a predetermined duration. In dynamic imaging, a gated method can be employed as in the cardiac blood pool gated studies, and in these studies, list mode acquisition of data is helpful providing very high temporal resolution. After acquisition, list mode data can be binned into sinograms, and frame durations can be determined. By reformatting a single list-mode acquisition into frames of different durations retains quantitative accuracy with respect to static frame data and compared to the known radionuclide concentration[10]. Whereas the static scans are useful to estimate the gross tracer uptake, dynamic scans provide information as to how the tracer distribution varies with time at a given site.

In frame mode or list mode, digitized signals are collected and stored in X, Y positions in a matrix of given size and depth for a specified time or total number of counts. In list mode, digitized X- and Y- signals are coded with "time marks" as they are received in sequence and stored as individual events as they occur. After the acquisition is completed, data can be manipulated to form images in a variety of ways to meet a specific need. This process is time consuming despite the wide flexibility it provides. In PET studies, while the frame mode acquisition has been routinely used, with the introduction of faster computers, the list mode acquisition is now being used more commonly for the newer cameras[11].

2.1.3 6-[^{18}F]Fluoro-L-DOPA (^{18}F-FDOPA)

Parkinson's disease is associated with a loss of dopamine-containing neurons in striatum of the brain. PD is caused by a shortage of dopamine. Dopamine, a neurotransmitter, plays an important role in the mediation of movement, cognition and emotion. Dopamine also plays a role in various neuropsychiatric disorders, such as schizophrenia, autism, attention deficit hyperactivity disorder, and drug abuse.

Dopamine is synthesized within nerve cells. L-tyrosine is converted to dihydroxyphenylalanine (L-DOPA) and then to dopamine in a two-step process. The first, rate limiting step is catalyzed by tyrosine 3-monoxygenase (tyrosine hydroxylase or TH). The second step is catalyzed by aromatic L-amino acid decarboxylase (L-DOPA decarboxylase, AAAD). In parts of the nervous system that release dopamine as a neurotransmitter (dopaminergic neurons), no further metabolism occurs and dopamine is stored in vesicles in the presynaptic nerve terminals by virtue of the dopamine reuptake transporter.

6-[^{18}F]Fluoro-L-DOPA (^{18}F-FDOPA) is a radiolabeled analog of L-DOPA used to evaluate the central dopaminergic function of pre-synaptic neurons using positron emission tomography (PET). FDOPA PET reflects DOPA transport into the neurons, DOPA decarboxylation and dopamine storage capacity. This tracer can access to bidirectional transport across the blood-brain barrier (BBB) by neutral amino acid carrier. The tracer is converted to 6-[^{18}F]fluorodopamine (FDA) by AAAD and retained in the striatum. FDA can be O-methylated by catechol-O-methyltransferase to 3-O-methyl-6-[^{18}F]fluoro-L-dopa (3-OMFD), which is uniformly distributed throughout the brain. FDA is also metabolized via monoamine oxidase to yield [^{18}F]6-fluoro-3,4-dihydroxyphenylacetic acid (FDOPAC) and subsequently by COMT to yield [^{18}F]6-fluorochomovanillic acid (FHVA), which in turn can cross the BBB and be cleared from tissue by venous blood flow. The schematic diagram of the various transport and biochemical pathways of FDOPA in the human body is illustrated in Figure 3. AAAD and COMT are also present in peripheral tissues such as liver, kidneys, and lung. In clinical studies, AAAD is commonly inhibited with carbidopa, whereas COMT is blocked by entacapone and nitecapone. These two types of inhibitors enhance the availability of FDOPA in the brain[12].

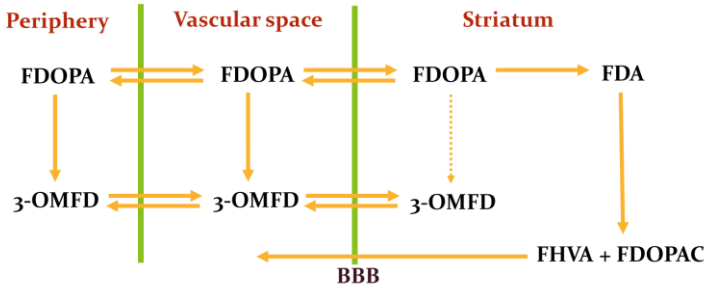

Figure 3 Schematic diagram illustrating the various transport and biochemical pathways of FDOPA in the human body.

2.1.4 ^{18}F-FDOPA PET Neuroimaging in PD

he first FDOPA PET study of human brain was reported in 1983, showing the localization of radioactivity in the striatum. Only about 1% of FDOPA entered the brain. Striatal-to-occipital ratio, FDOPA influx constant, and AAAD activity constant are commonly used as analytical parameters in FDOPA PET studies. In patients with established bilateral PD, FDOPA PET showed bilateral influx constant reductions in the caudate, putamen, striatal nigra, and midbrain tegmentum. The decline in FDOPA uptake was more rapid in PD than normal subjects. In PD patients, AAAD activity was reduced in striatum, putamen, and caudate and no change in frontal and occipital cortices[(12)].

In early hemiparkinsonian cases ^{18}F-FDOPA PET shows unilaterally reduced putamen tracer uptake (Figure 4Right), with activity being depressed in the caudal putamen contralateral to the affected limbs. PD patients with established disease show a 60-80% loss of specific putamen ^{18}F-FDOPA uptake in life, in line with the reported loss of ventrolateral nigra compacta cells but less than the 95% loss of putamen dopamine postmortem. These findings suggest that striatal dopamine terminal DOPA decarboxylase (DDC) activity may be relatively upregulated in PD, presumably to boost dopamine turnover by remaining neurons.

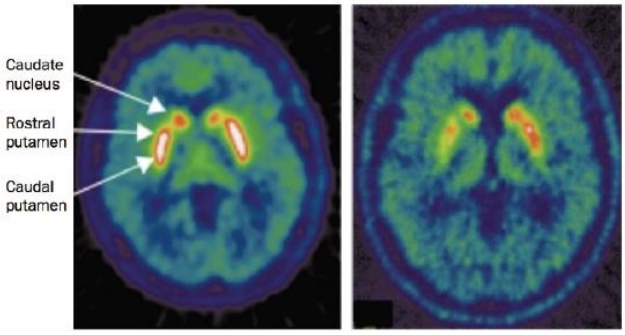

Figure 4 Transverse ^{18}F-FDOPA PET images of a healthy control (Left) and a patient with idiopathic PD (Right)[(13)].

It is known that the pathology of PD is not uniform and ventrolateral nigral dopaminergic projections to the dorsal putamen are more affected than dorsomedial projections to the head of caudate. ^{18}F-FDOPA PET reveals that in patients with unilateral PD (Hoehn and Yahr stage 1[(6)]) contralateral dorsal posterior putamen dopamine storage is first reduced. As all limbs become clinically affected, ventral and anterior putamen and dorsal caudate dopaminergic function also become involved. Finally, when PD is well advanced, the ventral head of caudate ^{18}F-FDOPA uptake starts to fall[(2)].

Not all dopamine fibers degenerate in early PD. Nigrostriatal projections comprise the densest dopamine pathway but there is also a nigro-internal pallidal pathway with 20% of their density. The striatum is the main input and the globus pallidus interna (GPi) is the main output nucleus of the basal ganglia, and the dopamine system modulates the function of both these structures. While putamen ^{18}F-FDOPA uptake is reduced by at least 30% at the onset of parkinsonian rigidity and bradykinesia, GPi ^{18}F-FDOPA uptake is initially increased by 40%. This increased uptake subsequently falls below normal levels as disease advances and loss of GPi ^{18}F-FDOPA upregulation coincides with the presence of fluctuating responses to levodopa, suggesting that both putamen and pallidum tonic dopamine release is required to facilitate fluent and efficient limb movements[13].

FDOPA PET permits objective monitoring of PD progression and neuroprotection therapies. It allows diagnosis of PD in early disease stages. In recent studies, FDOPA has also demonstrated its usefulness as in the imaging of brain tumors and neuroendocrine metastatic lesions in bone.

2.1.5 Kinetic Modeling in Positron Emission Tomography

Positron emission tomography (PET) is a functional imaging technique that enables not only visualization of the distribution of radiotracer, but also has ability to quantify several biomedical functions. Thus, given a time sequence of PET images, one can quantify tracer kinetics in vivo. The power of PET lies in its molecular specificity. By using a particular radiotracer molecule, one can monitor the interaction of that molecule with the body's physiological processes. With the acquisition of dynamic (time-sequence) imaging data and the application of kinetic models, one can pose many additional quantitative questions based on temporal information[14, 15].

In PET, the images are a composite of various superimposed signals, only one of which is of interest. The desired signal may describe, for example, the amount of tracer trapped at the site of metabolism or tracer bound to a particular receptor. In order to isolate the desired component of the signal, a mathematical model relating the dynamics of the tracer molecule and all its possible states to the resultant PET image are used. Each of these states is known in kinetic modeling as a compartment. A compartment may represent either a physical location where a substance resides or a specific chemical state of the substance under study[16]. Each compartment is characterized by the concentration of the tracer within it as a function of time compartment, given by C (e.g. expressed in $Bq.ml^{-1}$) and assumed that whatever radioactive species contribute to the emanating radioactive signal are in uniform concentration. These concentrations are related through sets of ordinary differential equations, which express the balance between the mass entering and exiting each compartment. By solving these simultaneous equations, the quantities of interest are determined[17].

Kinetic models for PET typically derive from the one-, two-, or three-compartment model in which a directly measured blood curve (concentration of radiotracer in the blood as a function of time) serves as the model's input function. The coefficients of the differential equations in the model are taken to be constants that are reflective of inherent kinetic properties of the particular tracer molecule in the system. The constants are typically called rate constant k which referred to rate of exchange of tracer between two compartments. By formally comparing the output of the model to the experimentally obtained PET data, the constant can estimate values for these kinetic parameters and thus extract information about binding, delivery, or any hypothesized process, as distinct from all other processes contributing to the PET signal. The kinetic modeling rate is measured in terms of perfusion of tissue, which is described as per unit time (min^{-1}) but the rate at which the tracer crosses the blood-brain barrier (BBB) to enter the first brain compartment is given by K_1. The K_1 rate constant only denoted in upper case and having units of ml plasma per gram per min ($ml.g^{-1}.min^{-1}$) to approximate blood flow for such tracers. This rate constant for blood-brain barrier transport is related to perfusion (blood flow), an example is shown as Figure 5.

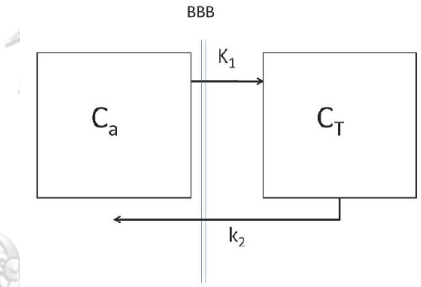

Figure 5 One-tissue compartment model[17].

2.1.6 Akaike's Information Criterion (AIC)

Akaike's information criterion (AIC) is a useful statistic for statistical model identification and evaluation. It compares the quality of a set of statistical models to each other. One of the main advantages of AIC lies in its simplicity which does not require any table lookup. There is no problem of subjectively specifying an arbitrary significance level to test the models, and comparisons are not restricted to two models which are nested or hierarchically ordered. It is easy to calculate AIC once the maximum likelihood estimators of the parameters of a model is determined. A model with a minimum value of AIC is chosen to be the best fitting model among several competing models[18, 19].

Akaike's Information Criterion is usually calculated with software. The basic formula is defined as:

$$AIC = -2(\text{log-likelihood}) + 2K$$

Where:

K is the number of model parameters (the number of variables in the model plus the intercept).

Log-likelihood is a measure of model fit. The higher the number, the better the fit. This is usually obtained from statistical output.

2.1.7 Bayesian Information Criterion (BIC)

In statistics, the Bayesian information criterion (BIC) or Schwarz criterion (also SBC, SBIC) is a criterion for model selection among a finite set of models. It is based, in part, on the likelihood function, and it is closely related to Akaike information criterion (AIC). When fitting models, it is possible to increase the likelihood by adding parameters, but doing so may result in overfitting. The BIC resolves this problem by introducing a penalty term for the number of parameters in the model. The penalty term is larger in BIC than in AIC[20].

The Bayesian Information Criterion (BIC) is defined as

$$BIC = k \log(n) - 2\log(L)$$

Where:

n = the number of data points in x, the number of observations, or equivalently, the sample size;

k = the number of free parameters to be estimated. If the estimated model is a linear regression, k is the number of regressors, including the intercept;

L = the maximized value of the likelihood function for the estimated model.

Given any two estimated models, the model with the lower value of BIC is the one to be preferred. Lower BIC implies either fewer explanatory variables, better fit, or both. The BIC generally penalizes free parameters more strongly than does the AIC, though it depends on the size of n and relative magnitude of n and k. It is important to keep in mind that the BIC can be used to compare estimated models only when the numerical values of the dependent variable are identical for all estimates being compared. The models being compared need not be nested, unlike the case when models are being compared using an F or likelihood ratio test[21].

2.2 Review of Related Literatures

Positron emission tomography (PET) of the brain has demonstrated distinct accumulation of radioactivity in regions with known dopaminergic neurotransmission following the administration of ^{18}F-FDOPA, an analogue of native L-DOPA. A variety of analytic methods have been developed to quantify ^{18}F-FDOPA PET images for the purpose of reliably discriminating patients with PD from healthy controls. However, only a few attempts have been made to measure the activity of DOPA decarboxylase by a model consistent with the underlying physiology and biochemistry of the dopaminergic system.

In 1991, Huang SC, et al[22] was likely the first group for studying the kinetics and modeling of L-6-[^{18}F] Fluoro-DOPA in human PET brain imaging based on compartmental model. Ten normal human subjects with PET from 0 to 120 min after an intravenous bolus injection of the ^{18}F-FDOPA tracer were measured and defined the time course of the arterial plasma concentrations of the tracer and its metabolites by biochemical assay. They suggested that a pharmacokinetics model consisting of three separate compartments for tissue FDOPA, tissue FDA and its metabolites, and tissue 3-OMFD, and 6 transfer rate constants could describe adequately the striatal kinetics in humans. Their FDOPA compartmental model is illustrated as in Figure 6.

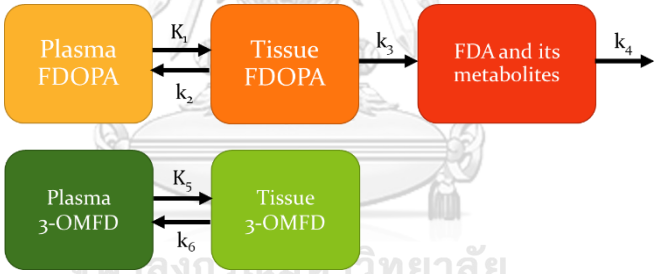

Figure 6 Compartmental model describing for the ^{18}F-FDOPA kinetics in Huang's study.

Another approach was proposed by Kuwabara, et al[23] in 1993. They studied in twelve healthy controls with PET acquired for 90 min following injection of ^{18}F-FDOPA. The compartment of FDA and its metabolites were separated into nondiffusible (mainly FDA) and diffusible compartments (FDOPAC and FHVA). Figure 7 depicts their compartmental model for tracer FDOPA. To improve the accuracy of the k_3 estimates, they estimated biological constraints which included a tracer partition volume (Ve) common to frontal cortex and striatum, and a fixed ratio (q) between the blood-brain barrier transport coefficients of OMFD and FDOPA. These values were used to construct the time course of FDOPA.

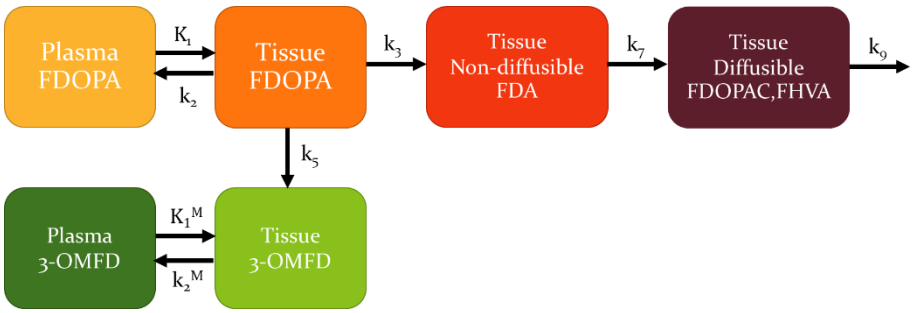

Figure 7 Compartmental model describing for the ^{18}F-FDOPA kinetics according to Kuwabara's study.

Later on, Wahl L and Nahmias C[24] studied modeling of Fluorine-18-6-Fluoro-L-Dopa in humans in 1996. The kinetics of ^{18}F-FDOPA in striatum were measured with PET from 0 to 150 min after an intravenous bolus injection of tracer in four normal subjects and two patients suffering from Parkinson's disease. On a separate occasion, the kinetics of OMFD was determined in the plasma and striatum of the same individuals. They found that the number of compartments and rate constants in compartmental analysis of the kinetics of ^{18}F-FDOPA could reduce into two-compartment, three-rate constant model (Figure 8).

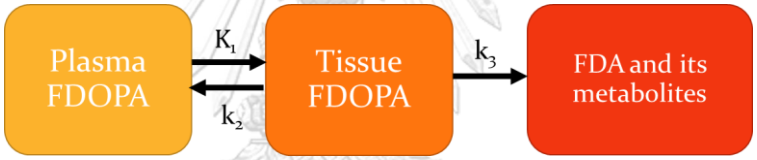

Figure 8 Compartmental model describing for the ^{18}F-FDOPA kinetics according to Wahl and Nahmias's study.

CHAPTER 3

RESEARCH METHODOLOGY

3.1 Research Design

This research was designed as an observational descriptive study in the type of retrospective to investigate patients' ^{18}F-FDOPA transfer rate constants. The procedures are as the following steps as by in the Figure 9.

3.2 Research Design Model

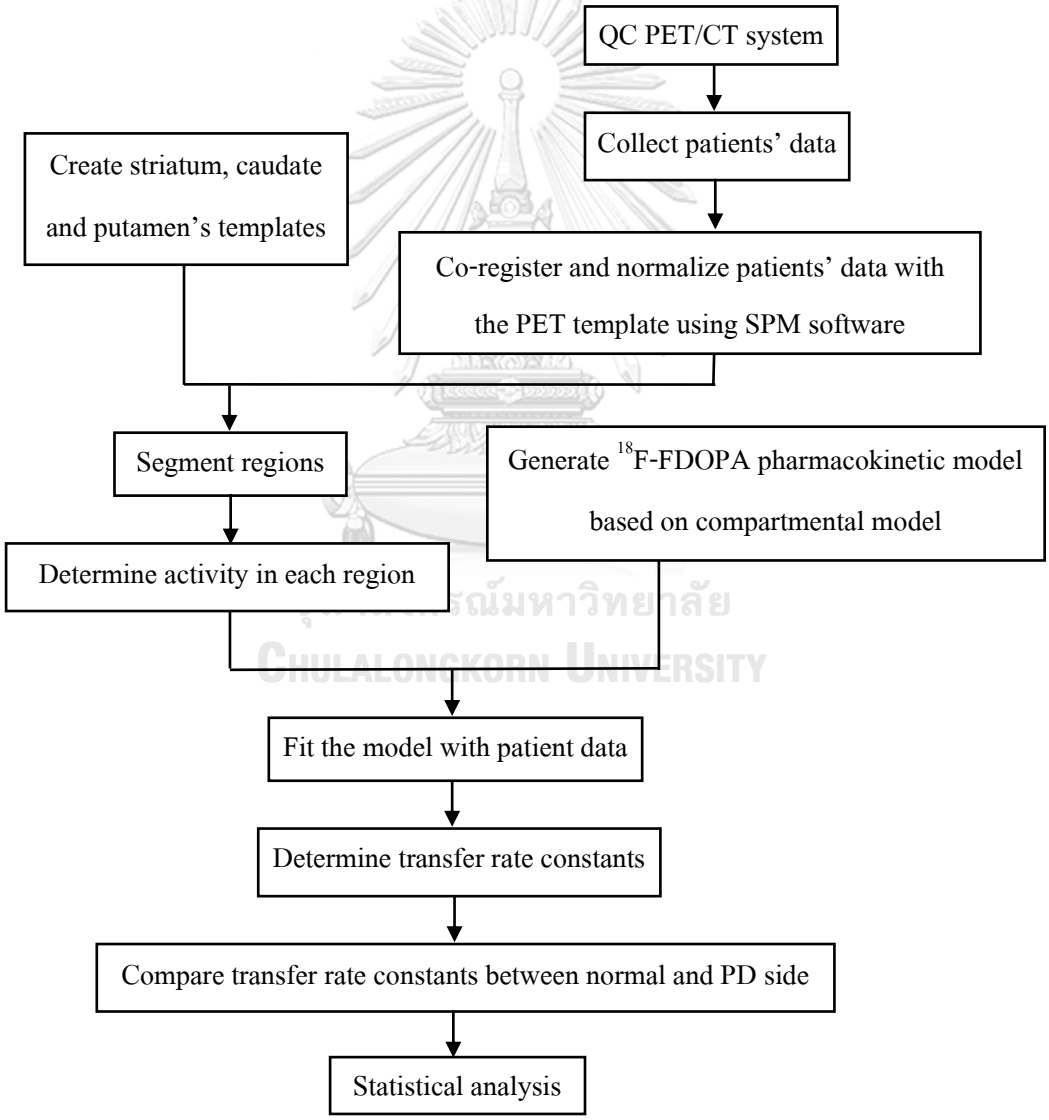

Figure 9 Research design model.

3.3 Conceptual Framework

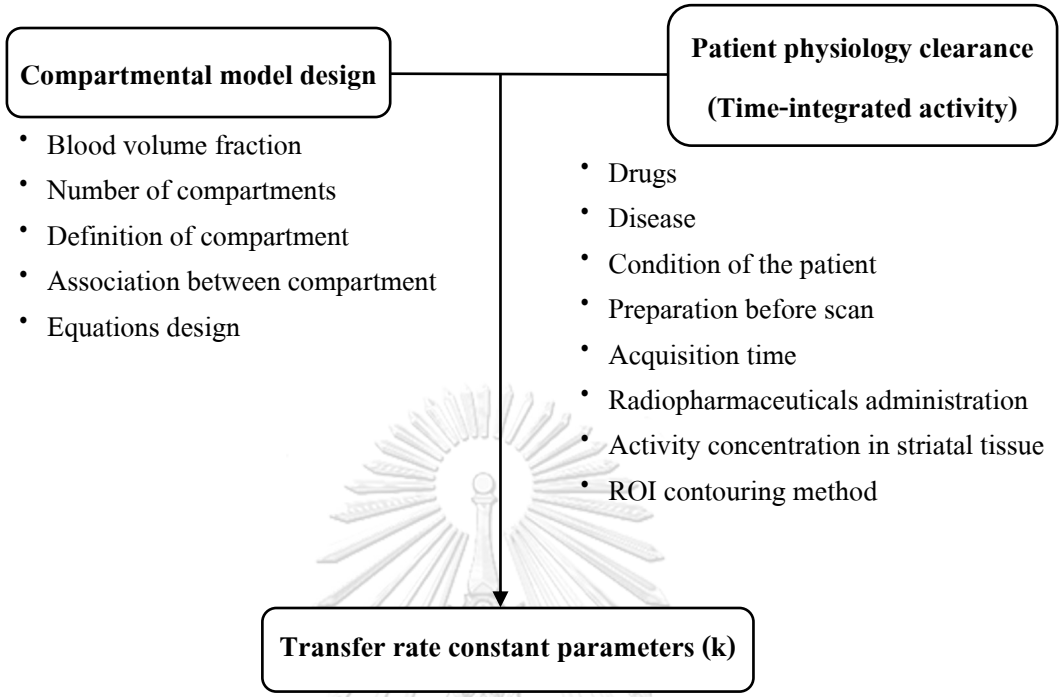

Figure 10 Conceptual framework.

3.4 Research Question

What are the transfer rate constants (k) of ^{18}F-FDOPA obtained in Thai early PD patients' brain based on compartmental model?

3.5 Key Words

PET/CT, ^{18}F-FDOPA, Parkinson's disease, Pharmacokinetic model, Statistical parametric mapping

3.6 The Sample

3.6.1 Target Population

All PET/CT images data set of early PD patients who underwent PET ^{18}F-FDOPA brain scan at Division of Nuclear Medicine, King Chulalongkorn Memorial Hospital.

3.6.2 Sample Population

The PET/CT images data set of early PD patients who underwent PET ^{18}F-FDOPA brain scan during year 2016 to 2018 at Division of Nuclear Medicine, King Chulalongkorn Memorial Hospital and met the eligible criteria.

3.6.3 Eligible Criteria

3.6.3.1 Inclusion Criteria

The patients who followed the UK Parkinson's Disease Society Brain Bank Clinical Diagnosis Criteria[25] and were diagnosed as PD stage I or II from the Hoehn and Yahr staging (HY staging)[6].

3.6.3.2 Exclusion Criteria

- Severe motion artifacts
- Drug-induced parkinsonian syndrome
- Vascular causes of parkinsonian syndrome

3.6.4 Sample Size Determination

The sample population is continuous, retrospective data and was determined by formula as following:

$$N = \frac{(Z\frac{\alpha}{2})^2 . \sigma^2}{d^2}$$

Where:

N = Sample size

$Z\alpha_{/2}$ = 95% Confidence Interval (1.96)

σ = Variance of data (0.0205)[24]

d = Acceptable error (0.02)

$$N = \frac{(1.96)^2 . 0.0205^2}{0.02^2}$$

Therefore: The sample size (N) for 95% confidence interval is 5 patients.

3.7 Materials

3.7.1 Positron Emission Tomography/Computed Tomography (PET/CT)

The PET/CT system at Division of Nuclear Medicine, King Chulalongkorn Memorial Hospital was used in this study as shown in Figure 11. The system is manufactured by Siemens Medical Solutions, Model Biograph Sensation 16 which integrates a PET scanner with a 16 multi-slice CT scanner. PET scanner consists of arrays of lutetium oxyorthosilicate (LSO) crystal detector with 4x4x20 mm dimension. The total numbers of LSO detectors are 24,336 detectors separated to 144 blocks and 169 crystals per block. The field of view (FOV) covers 162 mm in axial and 585 mm in transaxial.

Figure 11 PET/CT system model Siemens Biograph16.

3.7.2 Statistical Parametric Mapping (SPM)

The Statistical Parametric Mapping (SPM) software is available to the neuroimaging analysis. The software is generally used to identify functionally specialized brain responses and is the most prevalent approach to characterizing functional anatomy and disease-related changes. The alternative perspective, namely that provided by functional integration, requires a different set of multivariate approaches that examine the relationship among changes in activity in one brain area others. Statistical parametric mapping is a voxel-based approach, employing classical inference, to make some comment about regionally specific responses to experimental factors[26]. The SPM version 12 was used in this study as shown in Figure 12. The software operated on the MATLAB software version R2018a which is a high-level technical computing language and interactive environment for algorithm development, data visualization, data analysis, and numeric computation.

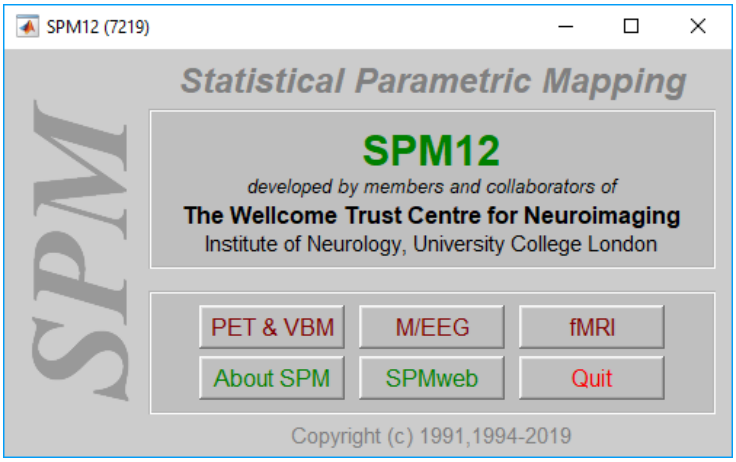

Figure 12 Statistical Parametric Mapping (SPM) software.

3.7.3 Image J

ImageJ is a public domain Java image processing program inspired by NIH Image for the Macintosh[27]. It runs, either as an online applet or as a downloadable application, on any computer with a Java 1.4 or later virtual machine. ImageJ can display, edit, analyze, process, save, and print 8-bit color and grayscale, 16-bit integer, and 32-bit floating point images. It can read many image file formats as well as raw formats. ImageJ can calculate area and pixel value statistics of user-defined selections and intensity-thresholded objects. It can measure distances and angles. It can also create density histograms and line profile plots. It supports standard image processing functions such as logical and arithmetical operations between images, contrast manipulation, convolution, Fourier analysis, sharpening, smoothing, edge detection, and median filtering.

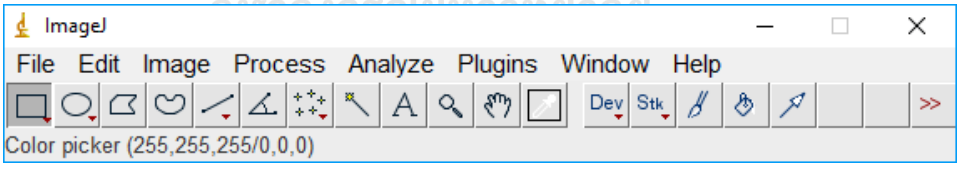

Figure 13 ImageJ.

3.7.4 SAAM II

SAAM II is a modeling, simulation, and analysis software package which supports the development and statistical calibration of compartmental models in biological, metabolic, and pharmaceutical systems. The users can define models, run simulations, and analyze results. SAAM II employs state-of-the-art numerical and statistical methods and algorithms. It is widely regarded as the most robust and accurate software package for solving systems of differential equations and for fitting model parameters to experimental data sets with specified (and flexible) error models[28].

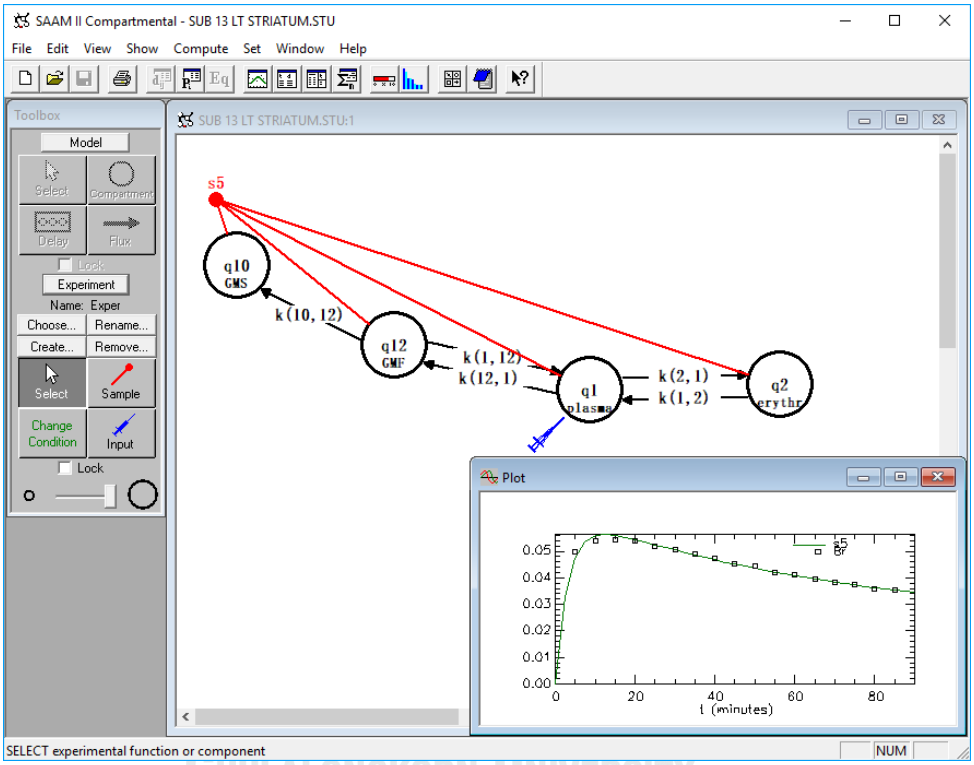

Figure 14 SAAM II.

3.8 Methods

This study was carried out as following:

3.8.1 PET/CT System Quality Control

The image quality control of PET/CT system was performed according to NEMA NU2-2007 protocol[29] by using an International Electric Commission (IEC) body phantom set as shown in Figure 15. [APPENDIX A]

Figure 15 Positioning of IEC body phantom for testing image quality of PET/CT system.

3.8.2 Patients Data Collection

This study was approved by the Institutional Review Board (IRB) of Faculty of Medicine, Chulalongkorn University (IRB no. 361/61) [APPENDIX B]. Five retrospective patients' data who underwent PET ^{18}F-FDOPA brain scan at Division of Nuclear Medicine, King Chulalongkorn Memorial Hospital (KCMH) and diagnosed as early Parkinson's disease were collected. The patient's data set were then extracted from the nuclear medicine PACS system. The information of the patient such as identification number, age, gender and injected activity were recorded in the case record form [APPENDIX C].

According to the clinical protocol at KCMH, antiparkinsonian drugs were discontinued 2 days before the examination. Patients were intravenously injected ^{18}F-FDOPA 5.55 MBq per kilogram. List-mode PET data was acquired immediately after injection for 90 min, and then followed by 30 min static images using the Biograph PET/CT system. A series of PET images were reconstructed with statistical iterative algorithms with 6 iterations and 16 subsets to obtain 5-min interval from 0 to 85-min time point. Decay correction, attenuation correction, and scatter correction was then applied for all reconstructed PET images. The examples of transaxial patient images of ^{18}F-FDOPA are shown in Figure 16.

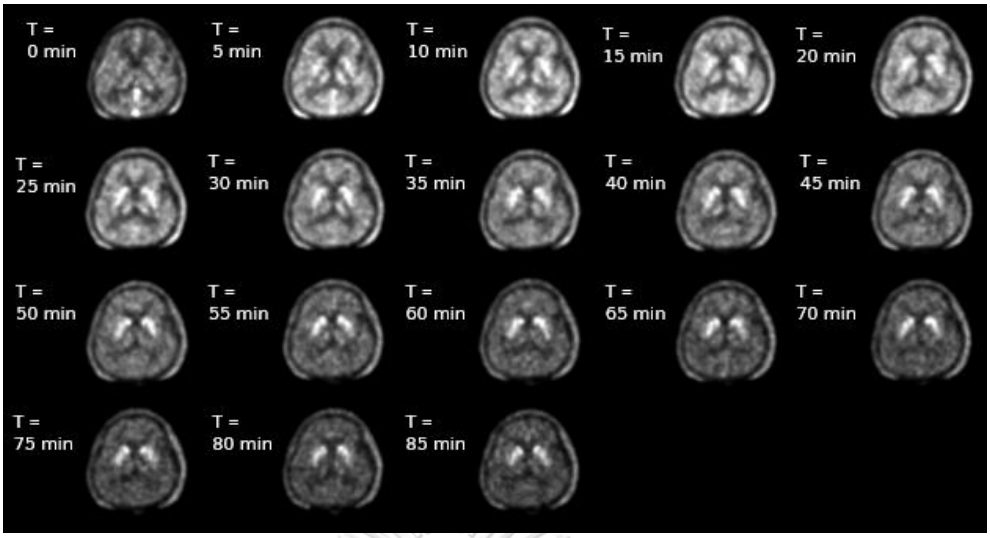

Figure 16 A series of PET images reconstructed with 5-min interval from 0 to 85-minute time points.

3.8.3 Automated Image Segmentation Using SPM

In order to keep the consistency and reliability of ROI contouring for striatum, caudate and putamen, all subsequent image manipulation and data analysis were performed on the Statistical Parametric Mapping (SPM) software version 12 which is operated based on the MATLAB software version R2018a. To generate the activity maps, the 5-minute interval list-mode PET images from 5 to 85-minute time point were used. The image segmentation in each time-point of patient data set was performed as following steps:

The image volumes of transverse slices were separated from the image headers using MRICRON software to make compatible with SPM. The images were then reoriented in SPM as closer as MRI referenced image as shown in Figure 17A by adjusting the individual movement parameters (pitch, roll, and yaw).

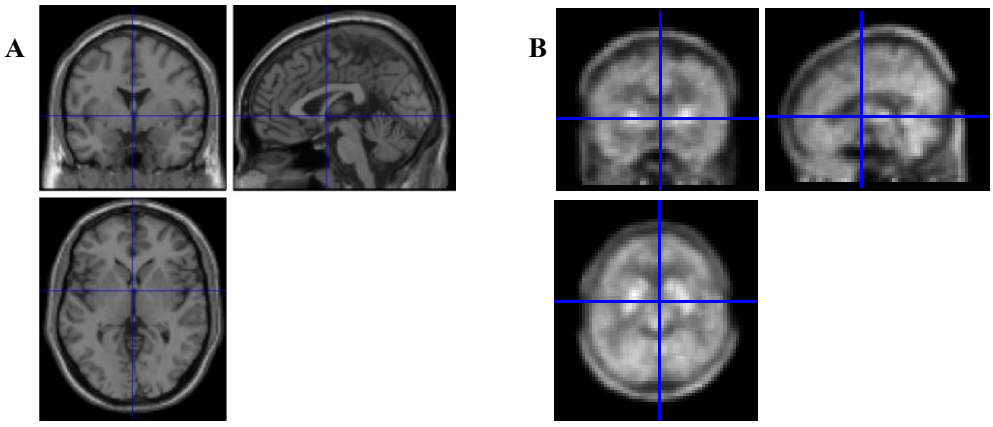

Figure 17 (A) MRI referenced image, and (B) PET reoriented images.

The PET reoriented images were within-subject registered using a rigid-body model or reference image which is the PET template (Figure 18B) that spatially normalized to International Consortium for Brain Mapping (ICBM). At the end of co-registration, the voxel-to-voxel affine transformation matrix was displayed, along with the histograms for the images in the original orientations, and the final orientations as shown in Figure 18A. The registered images are displayed in Figure 18C.

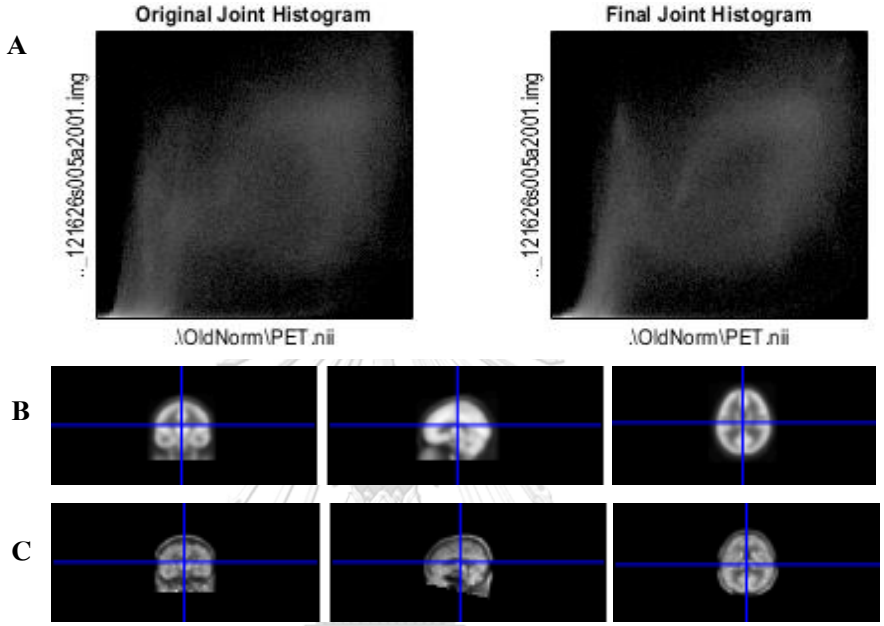

Figure 18 (A) the histograms for the images in the original orientations, and the final orientations, (B) the PET reference image, and (C) PET registered images.

The registered images were subsequently computed the warp that best register to match a PET template using Old normalize: estimate tool. ICBM space template affine regularization was used for making the warp more robust. Sixteen of iterations of nonlinear warping were performed with 25 of nonlinear frequency cutoff. The templates supplied with SPM have been smoothed by 8mm full-width at half maximum (FWHM) Gaussian filter, therefore, a copy of the registered images was applied the same smoothness. With Old normalize: write tool, it allows previously estimated warps to be applied to series of images by trilinear interpolation. The bounding box was determined -90, -126, -82.5; 90, 90, 97.5 with 1, 1, 1 voxel size. Spatially normalized images are not modulated. The warped images preserve the intensities of the original images and were set origin at 91, 126, 72. The 16-bit final images format with a size of 181 x 217 x 181 as shown in Figure 19B.

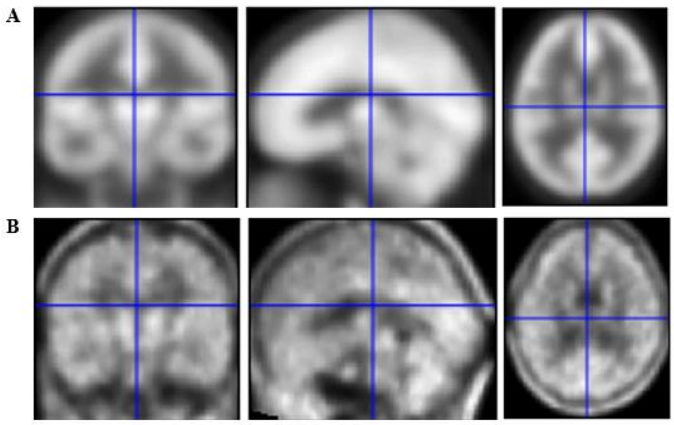

Figure 19 (A) The PET template, and (B) The normalized patient image.

We then created striatum, caudate and putamen templates which are generic VOIs by making a binary mask image of interested regions derived from the Automated Anatomical Labeling (AAL) software (i1) using Image Calculator. The algebraic expression which is a standard MATLAB expression was evaluated to extract selected regions as shown in Table 2. The numbers in the expression represent each region of the brain following the list of AAL brain structure definition. 71, 72, 73, and 74 portray as left and right of caudate and putamen respectively.

Table 2 The expression of each template.

Template	Expression
Striatum	(i1==71)+(i1==72)+(i1==73)+(i1==74)>0
Caudate	(i1==71)+(i1==72)>0
Putamen	(i1==73)+(i1==74)>0

The segmentation can be done by masking a bias corrected version, which can be generated by the segmentation option. This masking can be done using Image Calculator as well, by selecting the bias corrected scan (normalized images as i1), and the tissue class images (striatum, caudate, or putamen template as i2) and evaluating "i1.*i2" that the first image is used to make the mask, which is applied to the second image. The segmented striatum is illustrated as right lower of Figure 20. The segmented striatum, caudate, and putamen of each time point (Figure 21) were generated in every patient.

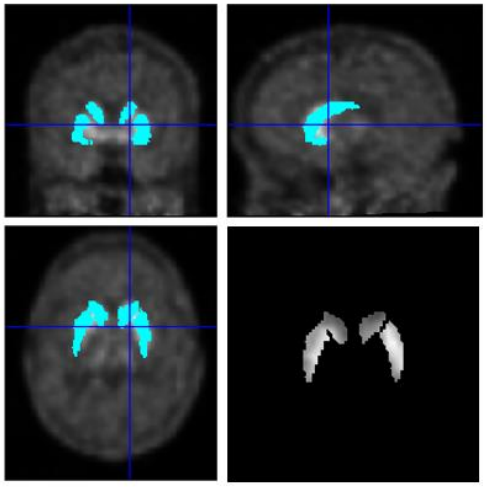

Figure 20 The superimposing of normalized patient images and striatum template (cyan color) in coronal, sagittal, and transverse planes. (Right lower) The final result image of striatum segmentations using the SPM.

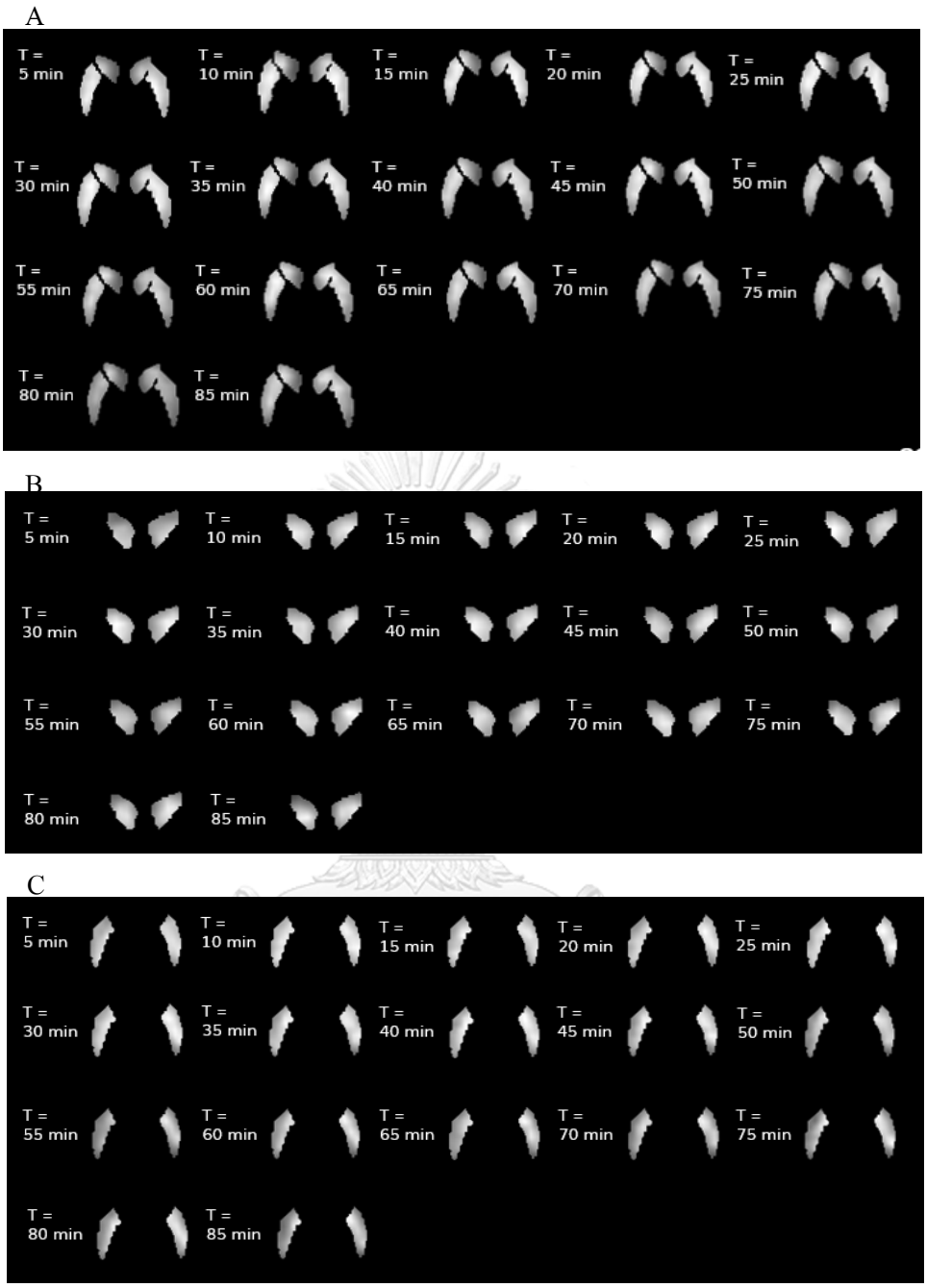

Figure 21 The segmented striatum (A), caudate (B) and putamen (C) in every time points.

3.8.4 Activity Concentration Measurement

According the co-registration and normalization, the changes of pixel values during SPM processing may occur between the original and normalized images (Figure 22). The whole-images histogram was computed in each time point using ImageJ program. The histogram provided mean and count values which refer to activity concentration (Bq/ml) and total number of voxels respectively. By multiplying these values and voxel volume (0.0248 ml in the original images, 0.001 ml in the normalized images), the whole-images activity (Bq) in each time points were determined. The whole-images activity from original images in each time point was then divided its own from normalized images then find mean value from every time point. The scaling factors were computed accordingly.

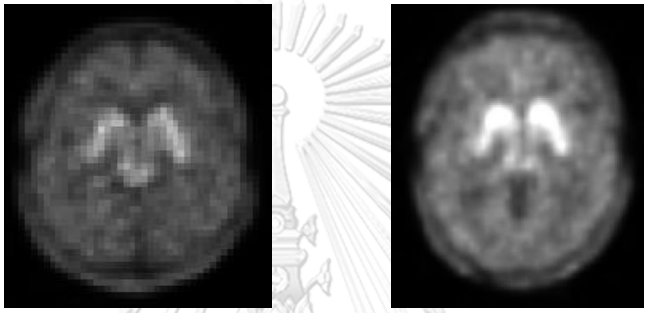

Figure 22 (Left) The original image, and (Right) The normalized image.

The regions of interest (ROI) were manually drawn over one side of the segmented striatum, caudate or putamen (Figure 23A) and also computed the histogram using ImageJ program (Figure 23B).

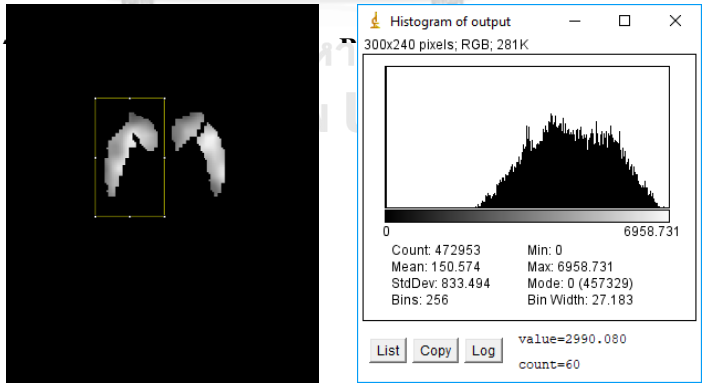

Figure 23 (A) ROI over one side of the segmented striatum, and (B) the histogram.

By multiplying activity concentration (Bq/ml), total number of voxels, voxel volume (0.001 ml) and the mean scaling factor, the whole-region activity (Bq) of striatum, caudate and putamen of each side in every time points were determined.

As the analysis of control and PD were performed within the same patient, all of the results were calculated separately for brain regions ipsilateral and contralateral to the side with predominant symptoms. We considered that contralateral side of patient's striatum, caudate or putamen which had lower uptake was PD and the ipsilateral side was control. As illustrated in Figure 24, there is slightly decreased ^{18}F-FDOPA uptake at left putamen which contralateral to side patient's predominant symptoms (right hand tremor and arm swing).

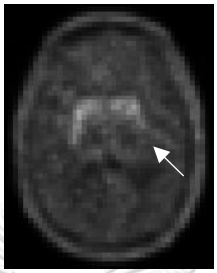

Figure 24 PET ^{18}F-FDOPA brain scan, (arrow) lower uptake at left putamen.

3.8.5 ^{18}F-FDOPA Pharmacokinetic Modeling for PD Patients

The activity of each side was calculated into percent injected activity as a function of time after injection. As a result, the FDOPA pharmacokinetic model was created using the SAAM II simulation program based on three-compartmental model to estimate transfer rate constants according to Wahl & Nahmias's model as shown in Figure 25. The movement of substances between the compartments is given by the following set of differential equations. The equations in each compartment were created internally and solved by SAAM II.

$$\frac{dCplasma\,(t)}{d(t)} = -K_1C_{plasma}(t) + k_2C_{Tissue}(t)\,d(t)$$

$$\frac{dCTissue\,(t)}{d(t)} = K_1C_{plasma}(t) - k_2C_{Tissue}(t) - k_3C_{Tissue}(t)$$

$$\frac{dC\,FDA(t)}{d(t)} = k_3C_{Tissue}(t)$$

where C_{plasma}, C_{Tissue}, and C_{FDA} represent radioactivity concentrations of the plasma FDOPA, tissue FDOPA, and FDA and its metabolites compartment respectively. K_1 and k_2 are the forward and reverse transport rate constants of plasma FDOPA across the blood brain barrier to the tissue FDOPA compartment, k_3 represents the FDOPA decarboxylation rate constant from the tissue FDOPA compartment to the combined compartment of FDA and its metabolites.

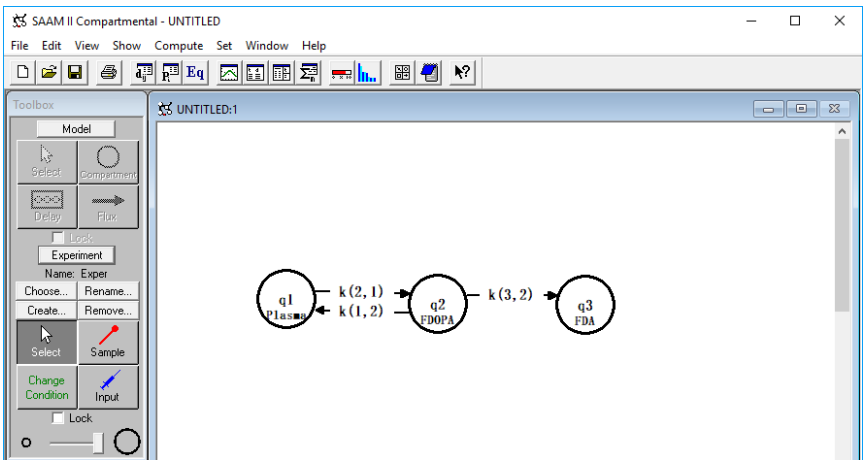

Figure 25 Compartmental model describing the kinetics of ^{18}F-FDOPA for PD patients in SAAM II.

Percent injected activities and time points from 5 to 85-minute time points were entered in input data of SAAMII simulation software as shown in Figure 26. For the model fitting, we performed using brain FDOPA exchange values initially obtained from Wahl and Nahmias then solved the system of differential equations represented by the compartmental model.

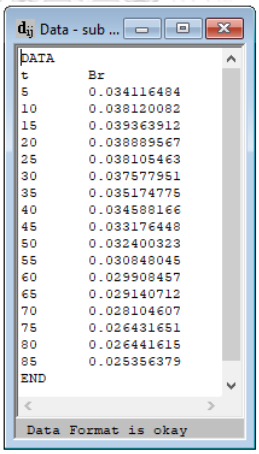

Figure 26 Percent injected activities were input into SAAM II.

The SAAM II software will then generate time-integrated activity curve of the model fitted to the patient data based on a nonlinear least square regression algorithm. The transfer rate constants (K_1, k_2 and k_3) in each patient were determined accordingly and compared between control and PD side of striatum, caudate and putamen. The Akaike information criterion (AIC) and Bayes information criterion were used to evaluate a relative goodness of model fitting.

3.9 Statistical Analysis

The transfer rate constants (K_1, k_2 and k_3) in each patient were determined accordingly and compared between normal and PD side of striatum, caudate and putamen using the non-parametric statistics, Wilcoxon signed rank test. Data analysis was done by using SPSS program, version 23.

3.10 Ethical Consideration

As the ^{18}F-FDOPA PET image data set of Parkinson's patients was investigated in this study, this research was approved by Institutional Review Board (IRB) of the Faculty of Medicine, Chulalongkorn University, Bangkok, Thailand (IRB No. 361/61). The certificate is shown in APPENDIX B.

3.11 Expected Benefits

To obtain the transfer rate constants from the biokinetic data of PET ^{18}F-FDOPA brain scan that can be used as an initial reference report for PD in Thai patients and provide quantitative medical tools to improve clinical PD diagnosis.

CHAPTER 4

RESULTS

4.1 Quality Control of PET/CT System

The quality control of PET/CT program was evaluated in terms of image quality, accuracy of attenuation and scatter correction. The results are shown in APPENDIX A.

4.2 Biodistribution Data of ^{18}F-FDOPA

PET ^{18}F-FDOPA brain images from 5 early PD patients were measured activity at striatum, caudate and putamen. The percent injected time-activity curve was used as the input function of the compartmental model to estimate transfer rate constants in each side of the regions. The characteristics of the enrolled patients' data are given in Table 3 and patient's PET ^{18}F-FDOPA brain images in every time points were shown from Figure 27 to 31. List-mode PET data was acquired immediately after injection for 90 min (17 time points) in every patient, except Patient no. 3 (Figure 29) that acquired only 85 min (16 time points).

Table 3 The clinical characteristics of five patients' data.

Characteristic	Patient 1	Patient 2	Patient 3	Patient 4	Patient 5	Mean ± SD
Age (years old)	63	64	62	44	71	60.8 ± 10.03
Sex	Male	Female	Female	Male	Female	
HY scale	II	II	II	II	II	
Lower uptake striatum	Left	Left	Left	Left	Left	
Injected activity (MBq)	301.07	305.58	322.46	379.62	349.28	331.60 ± 32.83

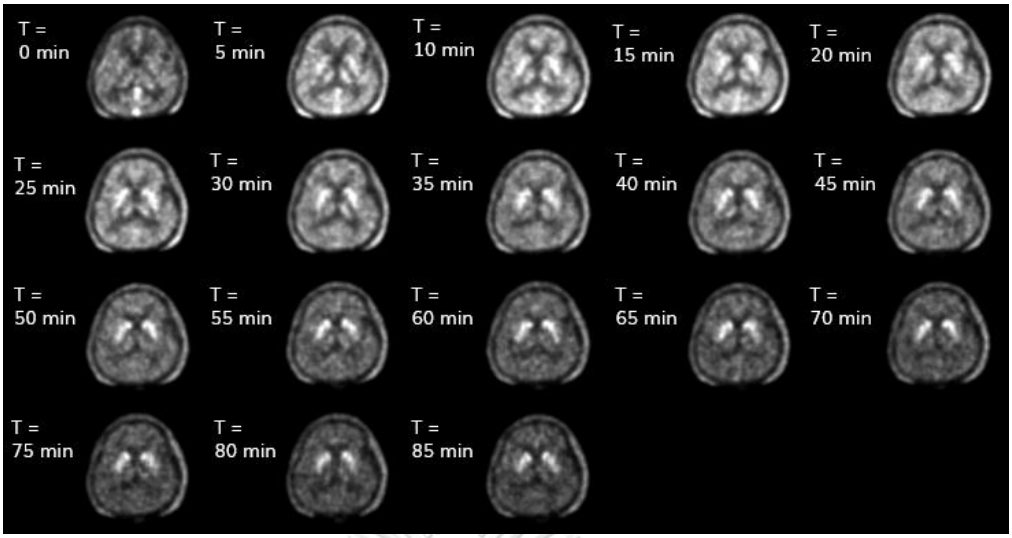

Figure 27 Patient 1's PET ^{18}F-FDOPA brain images in each time point.

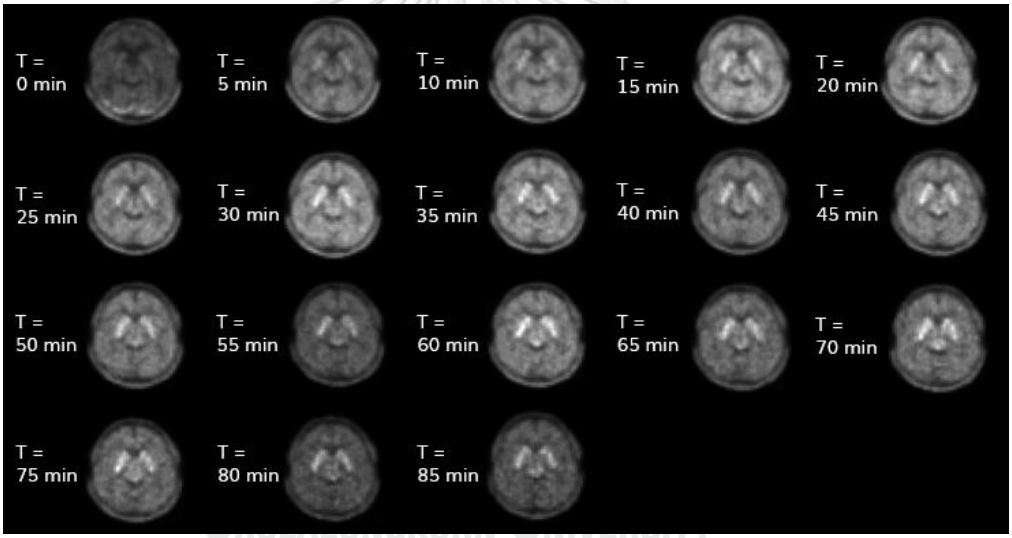

Figure 28 Patient 2's PET ^{18}F-FDOPA brain images in each time point.

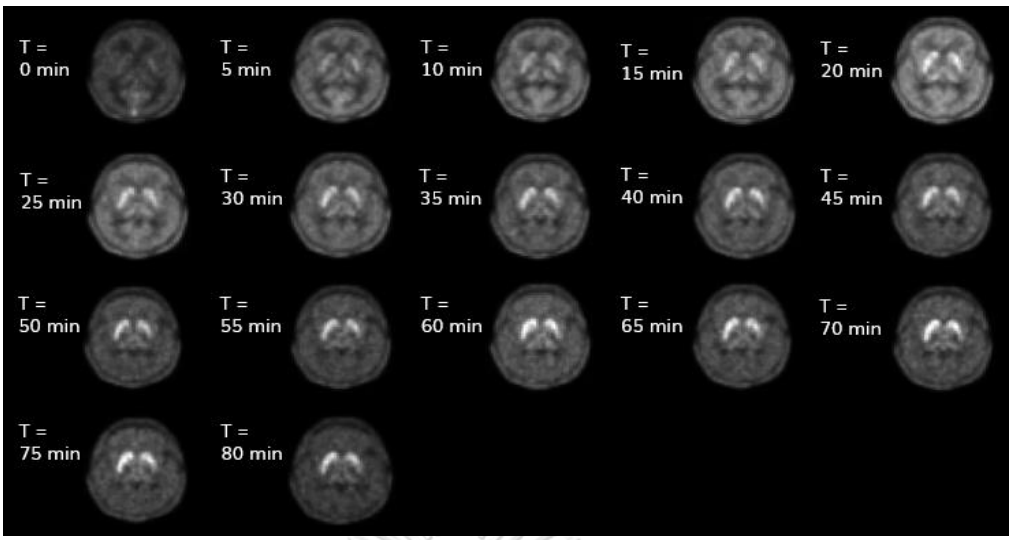

Figure 29 Patient 3's PET ^{18}F-FDOPA brain images in each time point.

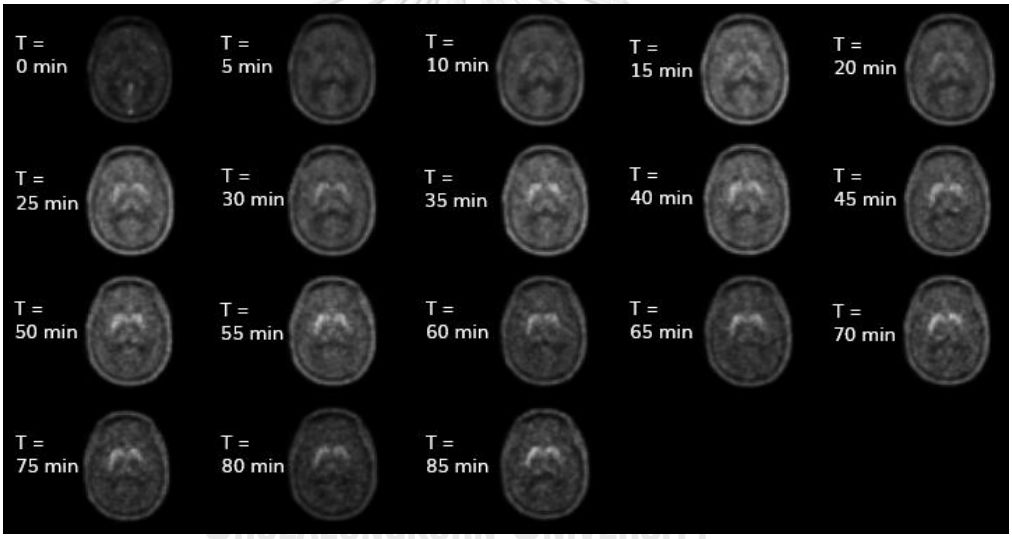

Figure 30 Patient 4's PET ^{18}F-FDOPA brain images in each time point.

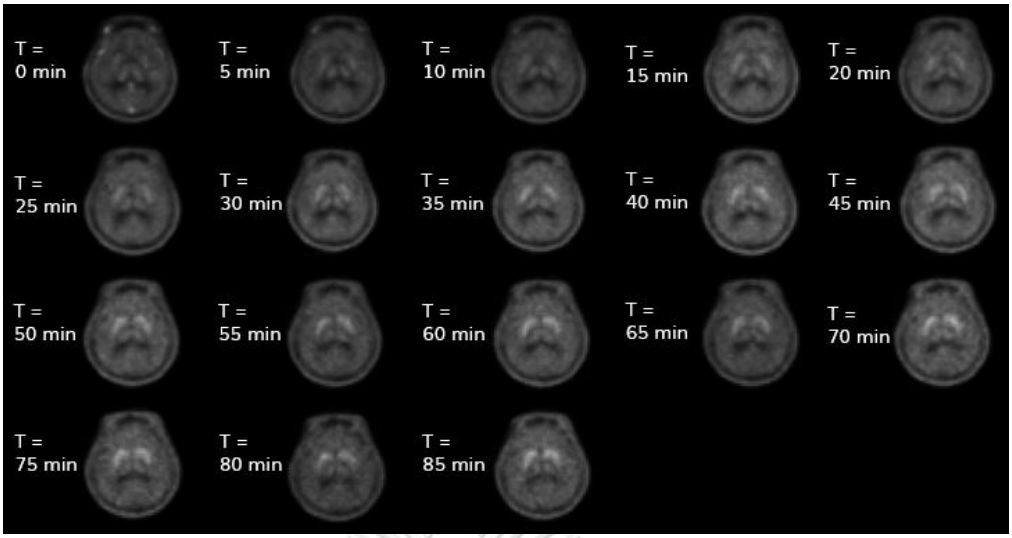

Figure 31 Patient 5's PET ^{18}F-FDOPA brain images in each time point.

All of the results were calculated separately for brain regions ipsilateral and contralateral according to the side with predominant symptoms. The activity uptake in the striatum, expressed as a percentage of injected activity, varied from 0.0225% to 0.0453% for contralateral side (Table 4 and Figure 32A) and from 0.0263% to 0.0457% for ipsilateral side (Table 5 and Figure 32B). For the caudate, percentage of injected activity ranged from 0.0112% to 0.0204% for contralateral side (Table 6 and Figure 33A) and from 0.0118% to 0.0191% for ipsilateral side (Table 7 and Figure 33B) were demonstrated. The percentage of injected activity in the putamen covered from 0.0113% to 0.0249% for contralateral side (Table 8 and Figure 34A) and from 0.0139% to 0.0273% for ipsilateral side (Table 9 and Figure 34B). The highest average percentages of injected activity in every region were at 15 min-time point and the lowest at 85 min-time point.

Table 4 Percentage of injected activity in contralateral striatum.

Time Point	Patient No.					Mean	SD
	1	2	3	4	5		
5	0.0248	0.0341	0.0381	0.0264	0.0500	0.0347	0.0101
10	0.0283	0.0381	0.0413	0.0290	0.0538	0.0381	0.0105
15	0.0289	0.0394	0.0424	0.0290	0.0545	0.0388	0.0106
20	0.0289	0.0389	0.0420	0.0281	0.0540	0.0384	0.0106
25	0.0284	0.0381	0.0412	0.0270	0.0520	0.0373	0.0102
30	0.0281	0.0376	0.0398	0.0260	0.0507	0.0364	0.0099
35	0.0277	0.0352	0.0383	0.0242	0.0490	0.0349	0.0097
40	0.0265	0.0346	0.0373	0.0236	0.0472	0.0338	0.0093
45	0.0260	0.0332	0.0362	0.0223	0.0453	0.0326	0.0090
50	0.0256	0.0324	0.0353	0.0207	0.0443	0.0317	0.0091
55	0.0245	0.0308	0.0342	0.0204	0.0419	0.0304	0.0084
60	0.0237	0.0299	0.0327	0.0191	0.0413	0.0293	0.0085
65	0.0229	0.0291	0.0324	0.0184	0.0393	0.0284	0.0081
70	0.0220	0.0281	0.0316	0.0179	0.0383	0.0276	0.0080
75	0.0215	0.0264	0.0309	0.0176	0.0375	0.0268	0.0078
80	0.0208	0.0264	0.0292	0.0171	0.0357	0.0258	0.0073
85	0.0220	0.0254	N/A	0.0165	0.0354	0.0248	0.0079
Mean	0.0253	0.0328	0.0364	0.0225	0.0453	0.0323	0.0091
SD	0.0028	0.0047	0.0043	0.0044	0.0067	0.0047	0.0011

Table 5 Percentage of injected activity in ipsilateral striatum.

Time Point	Patient No.					Mean	SD
	1	2	3	4	5		
5	0.0269	0.0372	0.0406	0.0286	0.0508	0.0368	0.0097
10	0.0289	0.0401	0.0439	0.0326	0.0541	0.0399	0.0099
15	0.0297	0.0424	0.0460	0.0326	0.0551	0.0412	0.0103
20	0.0306	0.0421	0.0471	0.0316	0.0539	0.0410	0.0100
25	0.0299	0.0404	0.0466	0.0309	0.0527	0.0401	0.0099
30	0.0304	0.0399	0.0455	0.0293	0.0510	0.0392	0.0094
35	0.0300	0.0386	0.0444	0.0280	0.0500	0.0382	0.0094
40	0.0296	0.0374	0.0434	0.0272	0.0472	0.0370	0.0086
45	0.0278	0.0365	0.0426	0.0263	0.0459	0.0358	0.0087
50	0.0272	0.0353	0.0414	0.0249	0.0442	0.0346	0.0085
55	0.0272	0.0343	0.0405	0.0238	0.0425	0.0337	0.0081
60	0.0267	0.0327	0.0400	0.0224	0.0416	0.0327	0.0083
65	0.0259	0.0324	0.0384	0.0228	0.0398	0.0319	0.0075
70	0.0252	0.0307	0.0381	0.0219	0.0385	0.0309	0.0075
75	0.0242	0.0300	0.0371	0.0217	0.0379	0.0302	0.0073
80	0.0238	0.0296	0.0363	0.0213	0.0367	0.0296	0.0070
85	0.0235	0.0289	N/A	0.0208	0.0357	0.0272	0.0066
Mean	0.0275	0.0358	0.0420	0.0263	0.0457	0.0353	0.0086
SD	0.0024	0.0045	0.0035	0.0042	0.0067	0.0044	0.0012

Table 6 Percentage of injected activity in contralateral caudate.

Time Point	Patient No.					Mean	SD
	1	2	3	4	5		
5	0.0108	0.0160	0.0173	0.0116	0.0219	0.0155	0.0045
10	0.0125	0.0185	0.0190	0.0137	0.0235	0.0174	0.0045
15	0.0132	0.0181	0.0198	0.0138	0.0237	0.0177	0.0044
20	0.0138	0.0183	0.0196	0.0136	0.0241	0.0179	0.0044
25	0.0138	0.0181	0.0201	0.0132	0.0227	0.0176	0.0041
30	0.0133	0.0180	0.0193	0.0124	0.0221	0.0170	0.0041
35	0.0140	0.0164	0.0192	0.0120	0.0215	0.0166	0.0038
40	0.0133	0.0163	0.0188	0.0119	0.0211	0.0163	0.0038
45	0.0125	0.0155	0.0183	0.0113	0.0198	0.0155	0.0036
50	0.0124	0.0156	0.0177	0.0104	0.0202	0.0153	0.0040
55	0.0126	0.0149	0.0176	0.0106	0.0192	0.0150	0.0035
60	0.0125	0.0142	0.0170	0.0098	0.0190	0.0145	0.0036
65	0.0120	0.0140	0.0169	0.0096	0.0182	0.0142	0.0035
70	0.0117	0.0134	0.0165	0.0095	0.0177	0.0138	0.0034
75	0.0115	0.0127	0.0162	0.0092	0.0177	0.0135	0.0034
80	0.0108	0.0128	0.0155	0.0089	0.0166	0.0129	0.0032
85	0.0112	0.0121	N/A	0.0089	0.0169	0.0123	0.0034
Mean	0.0125	0.0156	0.0181	0.0112	0.0204	0.0155	0.0038
SD	0.0010	0.0021	0.0014	0.0017	0.0025	0.0018	0.0004

Table 7 Percentage of injected activity in ipsilateral caudate.

Time Point	Patient No.					Mean	SD
	1	2	3	4	5		
5	0.0106	0.0161	0.0179	0.0124	0.0194	0.0153	0.0037
10	0.0120	0.0177	0.0195	0.0147	0.0209	0.0170	0.0036
15	0.0125	0.0189	0.0205	0.0150	0.0217	0.0177	0.0039
20	0.0131	0.0187	0.0214	0.0145	0.0211	0.0178	0.0038
25	0.0127	0.0178	0.0211	0.0146	0.0213	0.0175	0.0039
30	0.0127	0.0174	0.0204	0.0140	0.0208	0.0171	0.0037
35	0.0126	0.0172	0.0199	0.0132	0.0202	0.0166	0.0036
40	0.0126	0.0164	0.0199	0.0127	0.0191	0.0162	0.0034
45	0.0116	0.0165	0.0193	0.0124	0.0192	0.0158	0.0037
50	0.0114	0.0156	0.0189	0.0119	0.0182	0.0152	0.0035
55	0.0122	0.0145	0.0187	0.0113	0.0173	0.0148	0.0032
60	0.0119	0.0143	0.0185	0.0108	0.0167	0.0144	0.0032
65	0.0116	0.0142	0.0175	0.0108	0.0163	0.0141	0.0029
70	0.0110	0.0140	0.0177	0.0106	0.0156	0.0138	0.0030
75	0.0104	0.0131	0.0172	0.0105	0.0153	0.0133	0.0030
80	0.0108	0.0131	0.0172	0.0103	0.0151	0.0133	0.0029
85	0.0101	0.0130	N/A	0.0100	0.0145	0.0119	0.0022
Mean	0.0118	0.0158	0.0191	0.0123	0.0184	0.0154	0.0034
SD	0.0009	0.0020	0.0014	0.0017	0.0025	0.0018	0.0004

Table 8 Percentage of injected activity in contralateral putamen.

Time Point	Patient No.					Mean	SD
	1	2	3	4	5		
5	0.0140	0.0182	0.0208	0.0148	0.0281	0.0192	0.0057
10	0.0158	0.0205	0.0222	0.0154	0.0303	0.0208	0.0061
15	0.0158	0.0213	0.0226	0.0152	0.0308	0.0211	0.0063
20	0.0151	0.0206	0.0223	0.0145	0.0299	0.0205	0.0062
25	0.0146	0.0200	0.0210	0.0138	0.0293	0.0198	0.0062
30	0.0148	0.0196	0.0204	0.0135	0.0285	0.0194	0.0059
35	0.0137	0.0188	0.0190	0.0122	0.0274	0.0182	0.0060
40	0.0132	0.0182	0.0186	0.0117	0.0261	0.0175	0.0056
45	0.0134	0.0176	0.0179	0.0110	0.0256	0.0171	0.0055
50	0.0132	0.0168	0.0176	0.0103	0.0241	0.0164	0.0052
55	0.0119	0.0159	0.0166	0.0098	0.0227	0.0154	0.0050
60	0.0112	0.0157	0.0158	0.0094	0.0223	0.0149	0.0050
65	0.0109	0.0151	0.0155	0.0088	0.0211	0.0143	0.0047
70	0.0103	0.0147	0.0151	0.0084	0.0207	0.0138	0.0048
75	0.0100	0.0137	0.0147	0.0084	0.0198	0.0133	0.0044
80	0.0099	0.0136	0.0137	0.0082	0.0191	0.0129	0.0042
85	0.0109	0.0132	N/A	0.0076	0.0185	0.0126	0.0046
Mean	0.0129	0.0173	0.0184	0.0113	0.0249	0.0169	0.0054
SD	0.0020	0.0027	0.0030	0.0027	0.0042	0.0029	0.0007

Table 9 Percentage of injected activity in ipsilateral putamen.

Time Point	Patient No.					Mean	SD
	1	2	3	4	5		
5	0.0162	0.0212	0.0227	0.0162	0.0314	0.0215	0.0062
10	0.0170	0.0224	0.0245	0.0178	0.0331	0.0230	0.0065
15	0.0172	0.0235	0.0255	0.0177	0.0334	0.0234	0.0066
20	0.0174	0.0234	0.0256	0.0172	0.0328	0.0233	0.0065
25	0.0173	0.0226	0.0255	0.0164	0.0314	0.0226	0.0062
30	0.0177	0.0224	0.0252	0.0153	0.0302	0.0222	0.0059
35	0.0174	0.0214	0.0244	0.0147	0.0298	0.0216	0.0059
40	0.0170	0.0210	0.0235	0.0144	0.0280	0.0208	0.0053
45	0.0162	0.0201	0.0233	0.0139	0.0267	0.0200	0.0052
50	0.0158	0.0197	0.0225	0.0131	0.0260	0.0194	0.0052
55	0.0150	0.0197	0.0218	0.0125	0.0252	0.0188	0.0051
60	0.0148	0.0184	0.0215	0.0116	0.0248	0.0182	0.0053
65	0.0144	0.0182	0.0210	0.0119	0.0235	0.0178	0.0047
70	0.0141	0.0168	0.0204	0.0113	0.0229	0.0171	0.0046
75	0.0138	0.0170	0.0199	0.0113	0.0227	0.0169	0.0046
80	0.0131	0.0165	0.0191	0.0110	0.0216	0.0163	0.0043
85	0.0134	0.0160	N/A	0.0109	0.0212	0.0153	0.0044
Mean	0.0157	0.0200	0.0229	0.0139	0.0273	0.0199	0.0054
SD	0.0016	0.0025	0.0021	0.0025	0.0042	0.0026	0.0008

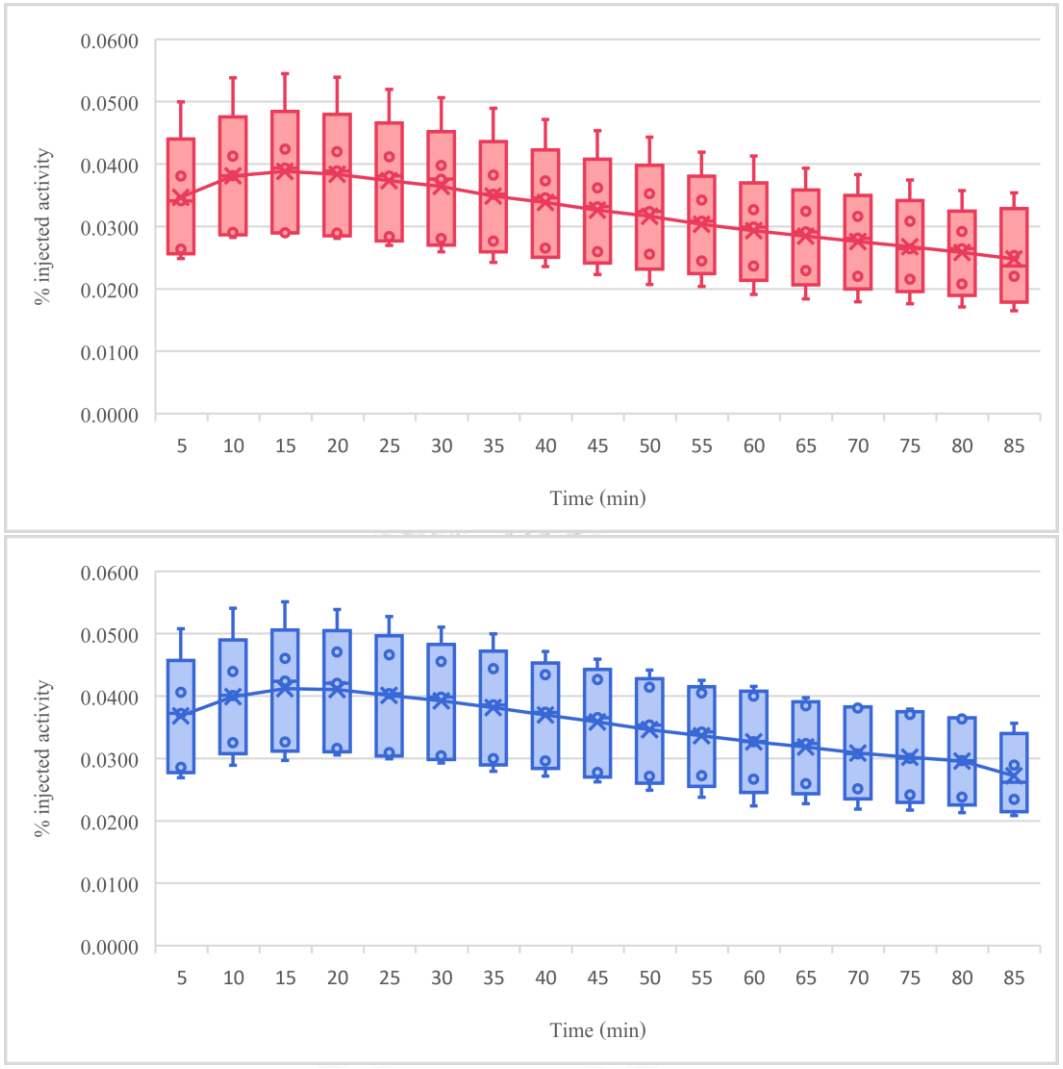

Figure 32 Box plots of percentage of injected activity in contralateral (upper) and ipsilateral (lower) striatum in each time point.

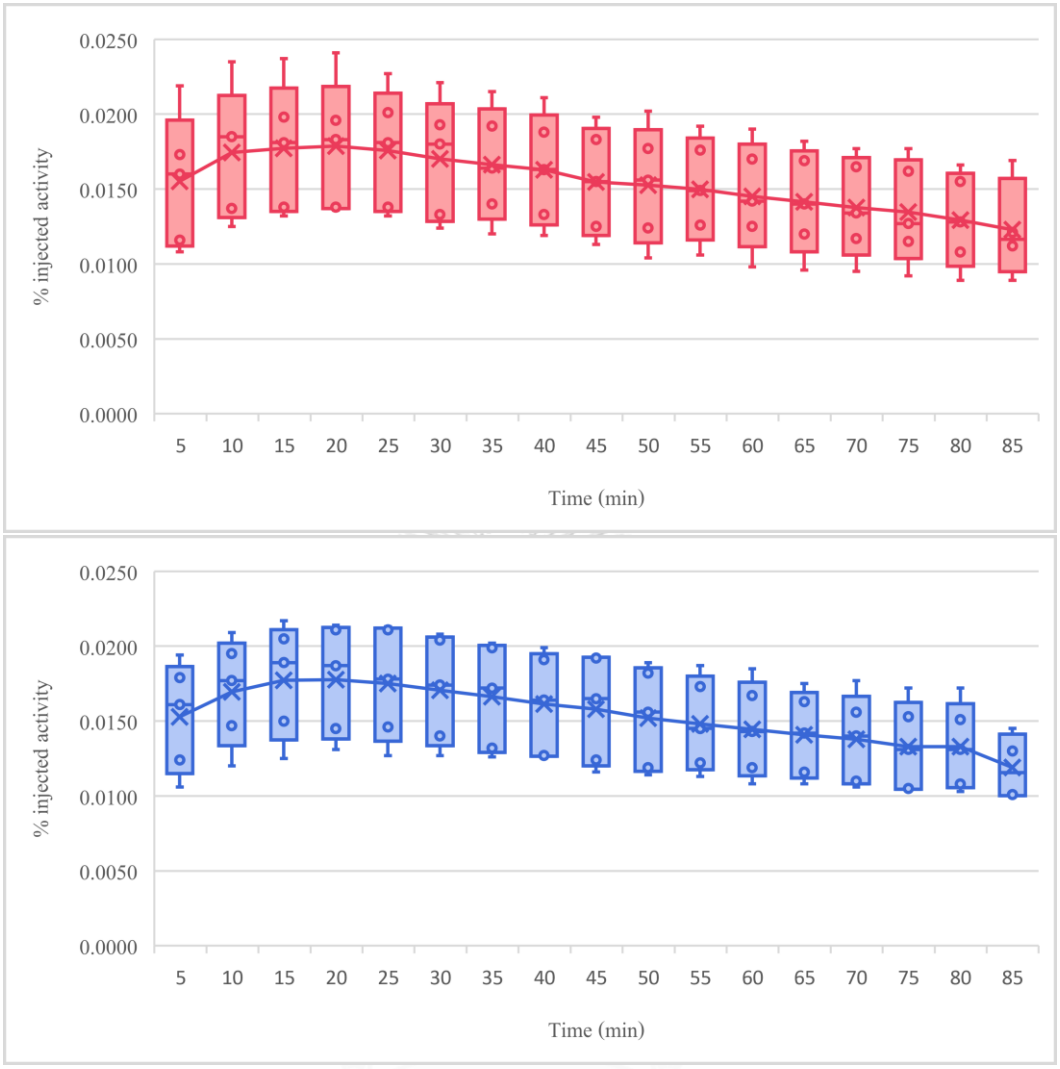

Figure 33 Box plots of percentage of injected activity in contralateral (upper) and ipsilateral (lower) caudate in each time point.

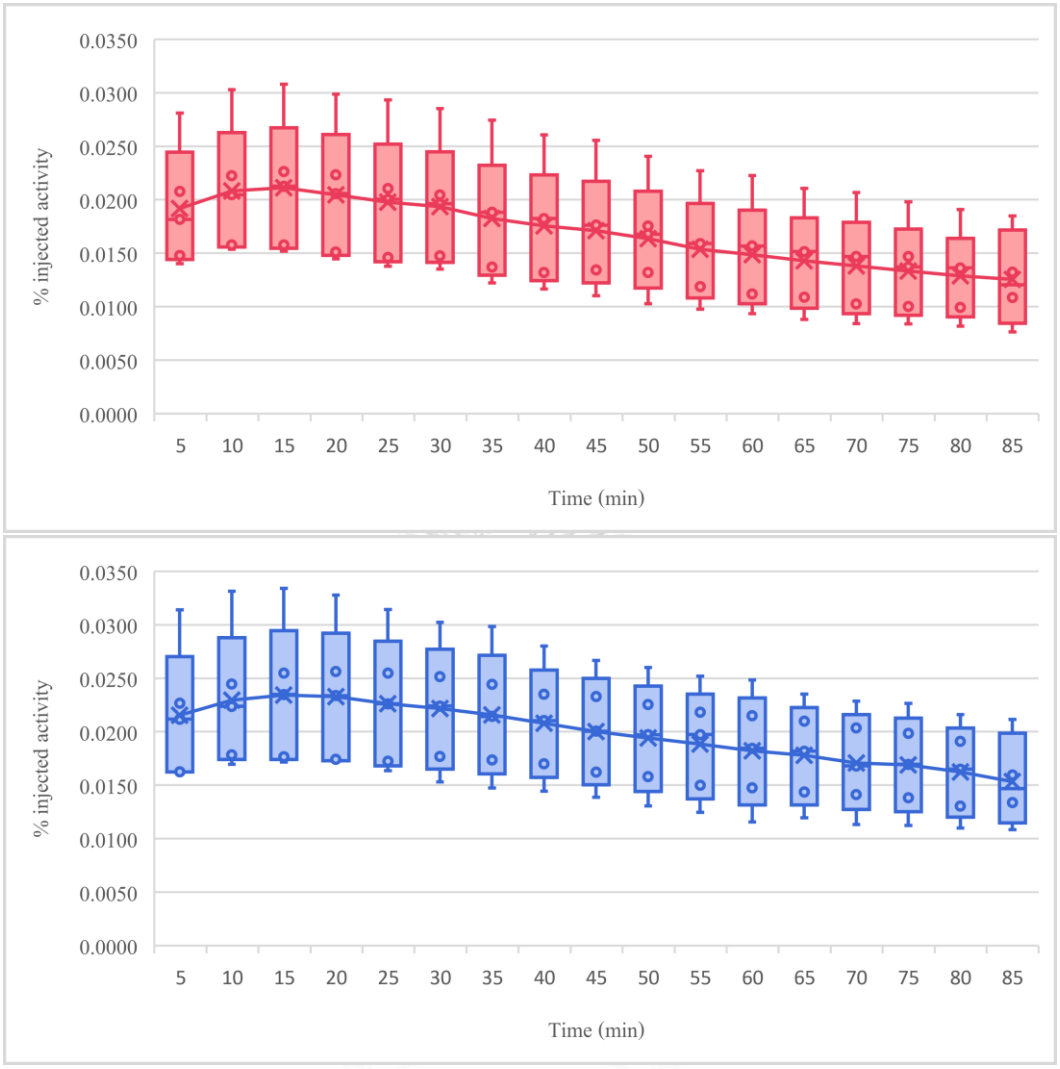

Figure 34 Box plots of percentage of injected activity in contralateral (upper) and ipsilateral (lower) putamen in each time point.

4.3 Biokinetic Data of ^{18}F-FDOPA

Figure 38 to 42 present every patients' time-activity curve in in both ipsilateral and contralateral side of striatum, caudate and putamen with simulated data from the model. The measured FDOPA curves were fitted well by a three-compartment, three-rate constant model. The simulated striatal time-activity curves in Patient no 1 (Figure 35A) were close each other with a little higher in the ipsilateral, which similar to the putamen (Figure 35C), the simulated time-activity curves have clearer difference. In contrast, the simulated time-activity curve in contralateral caudate (Figure 35B) was higher than the another. Both simulated striatal and putamen time-activity curves in Patient no 2 (Figure 36A, C), the ipsilateral was higher than the contralateral while the curves in caudate (Figure 36B) was overlay to each other. Patient no. 3 and 4 (Figure 37, 38) had similar trend of the simulated time-activity curves. The ipsilateral curves in every region were higher than the other side with clearest difference at putamen and following by striatum and caudate respectively. The simulated contralateral caudate time-activity curves in Patient no 5 (Figure 39B) was higher than the other side but was lower in putamen (Figure 39C) which resulted in superimposing curves in striatum (Figure 39A).

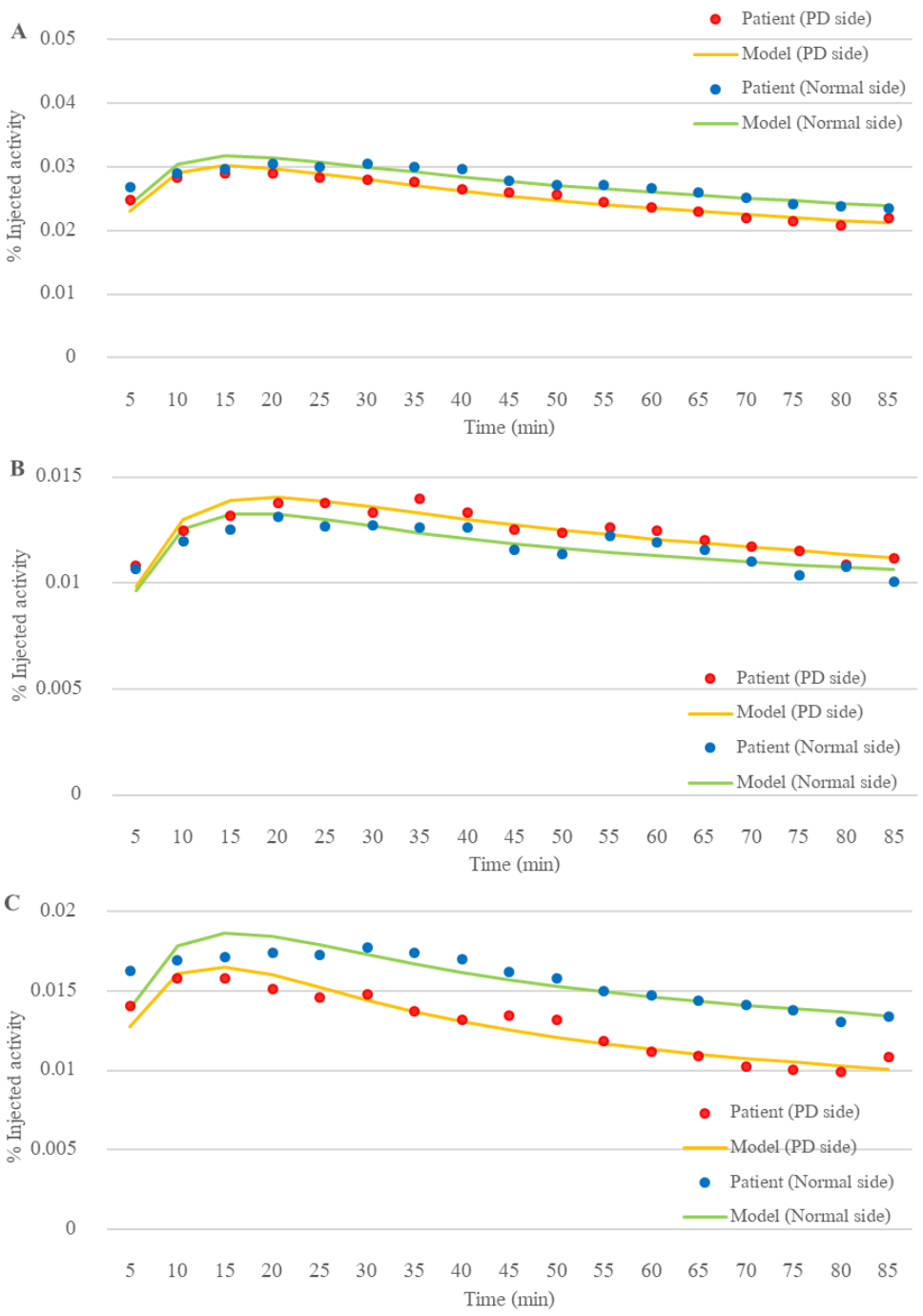

Figure 35 The Patient no 1's time-activity curves in the striatum (A), caudate (B) and putamen (C).

* Blue and red round markers represent patient's data obtained from contralateral and ipsilateral side respectively. Green and yellow lines represent the model fitted from contralateral and ipsilateral side respectively.

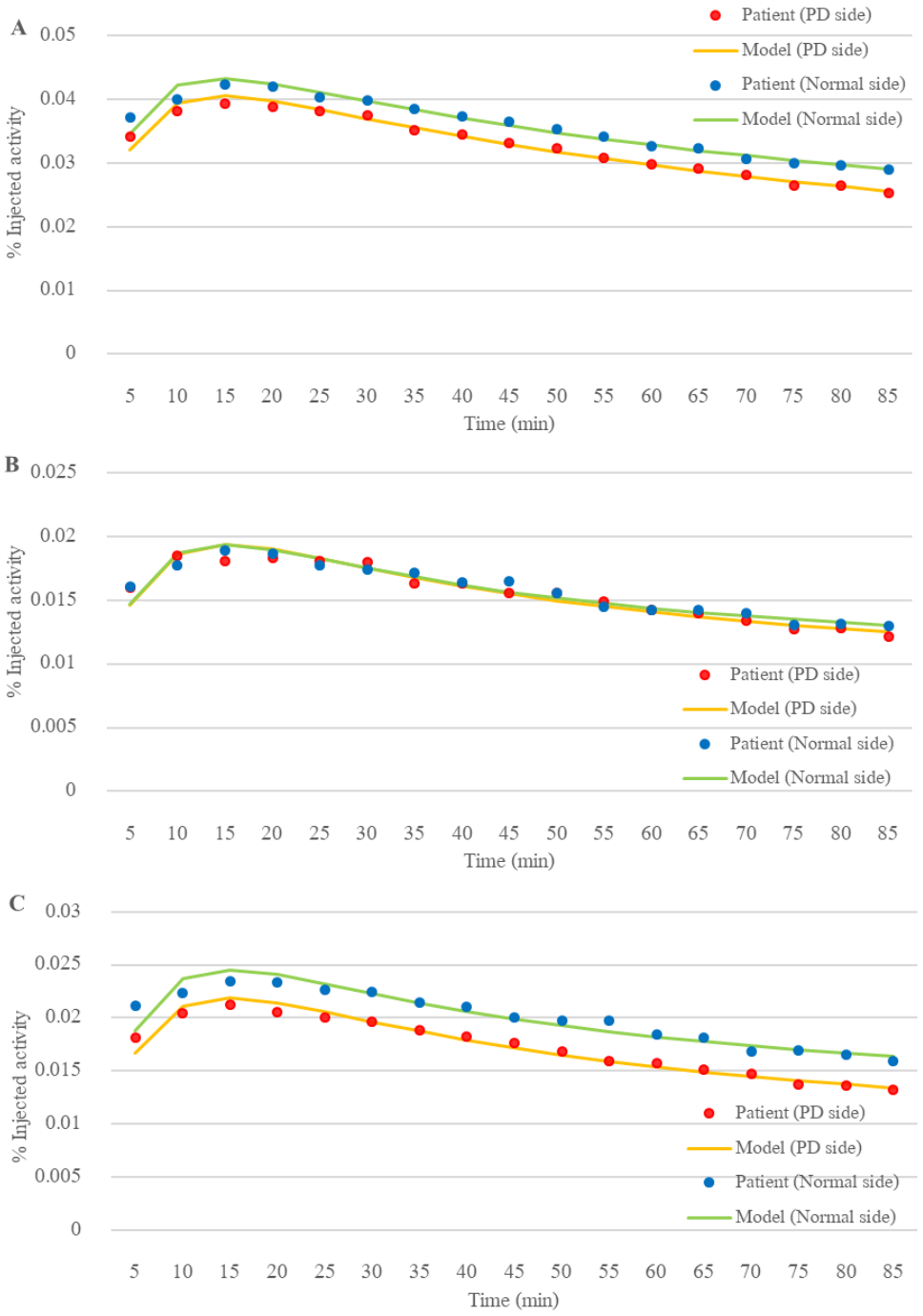

Figure 36 The Patient no 2's time-activity curves in the striatum (A), caudate (B) and putamen (C).

* Blue and red round markers represent patient's data obtained from contralateral and ipsilateral side respectively. Green and yellow lines represent the model fitted from contralateral and ipsilateral side respectively.

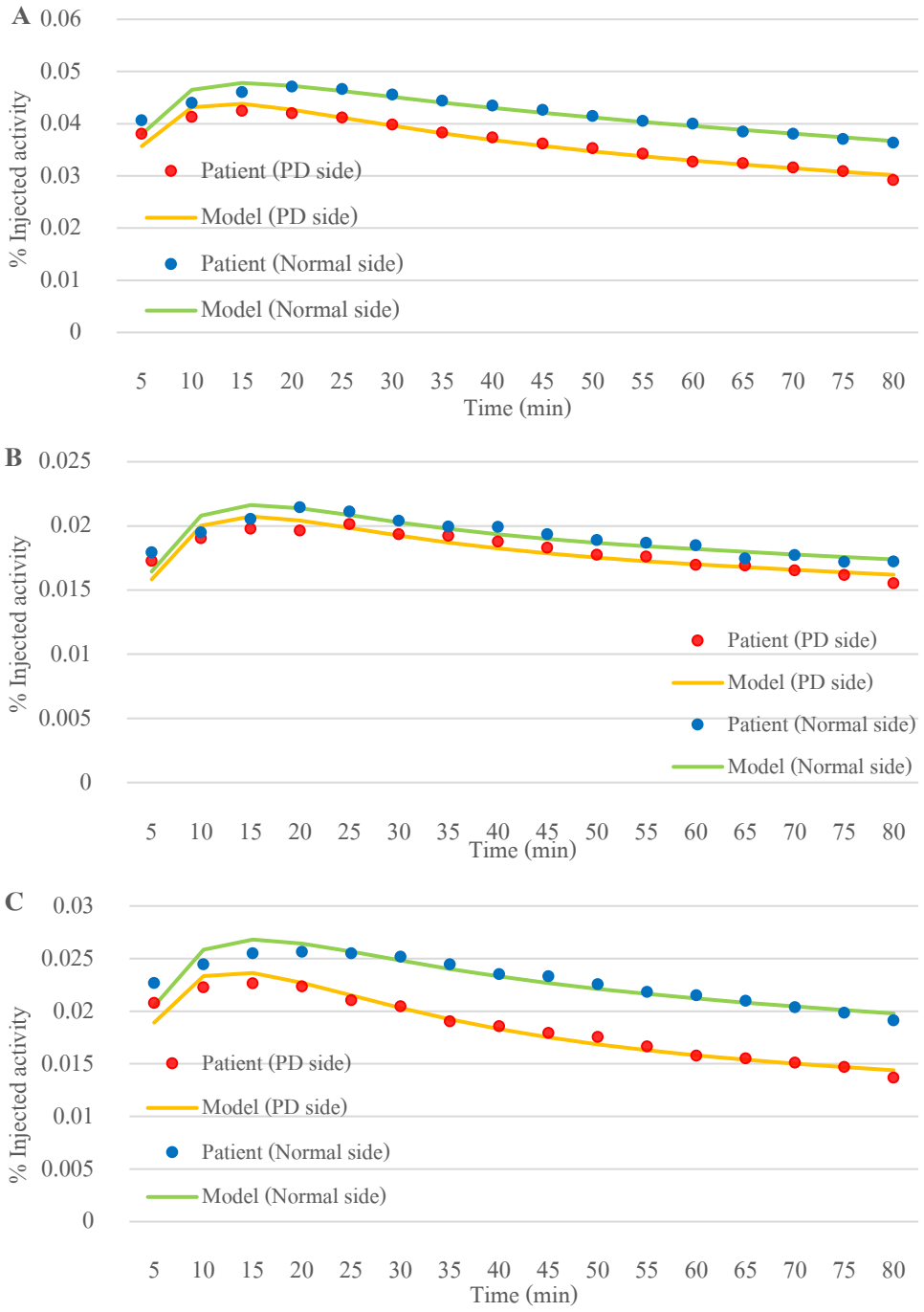

Figure 37 The Patient no 3's time-activity curves in the striatum (A), caudate (B) and putamen (C).

* Blue and red round markers represent patient's data obtained from contralateral and ipsilateral side respectively. Green and yellow lines represent the model fitted from contralateral and ipsilateral side respectively.

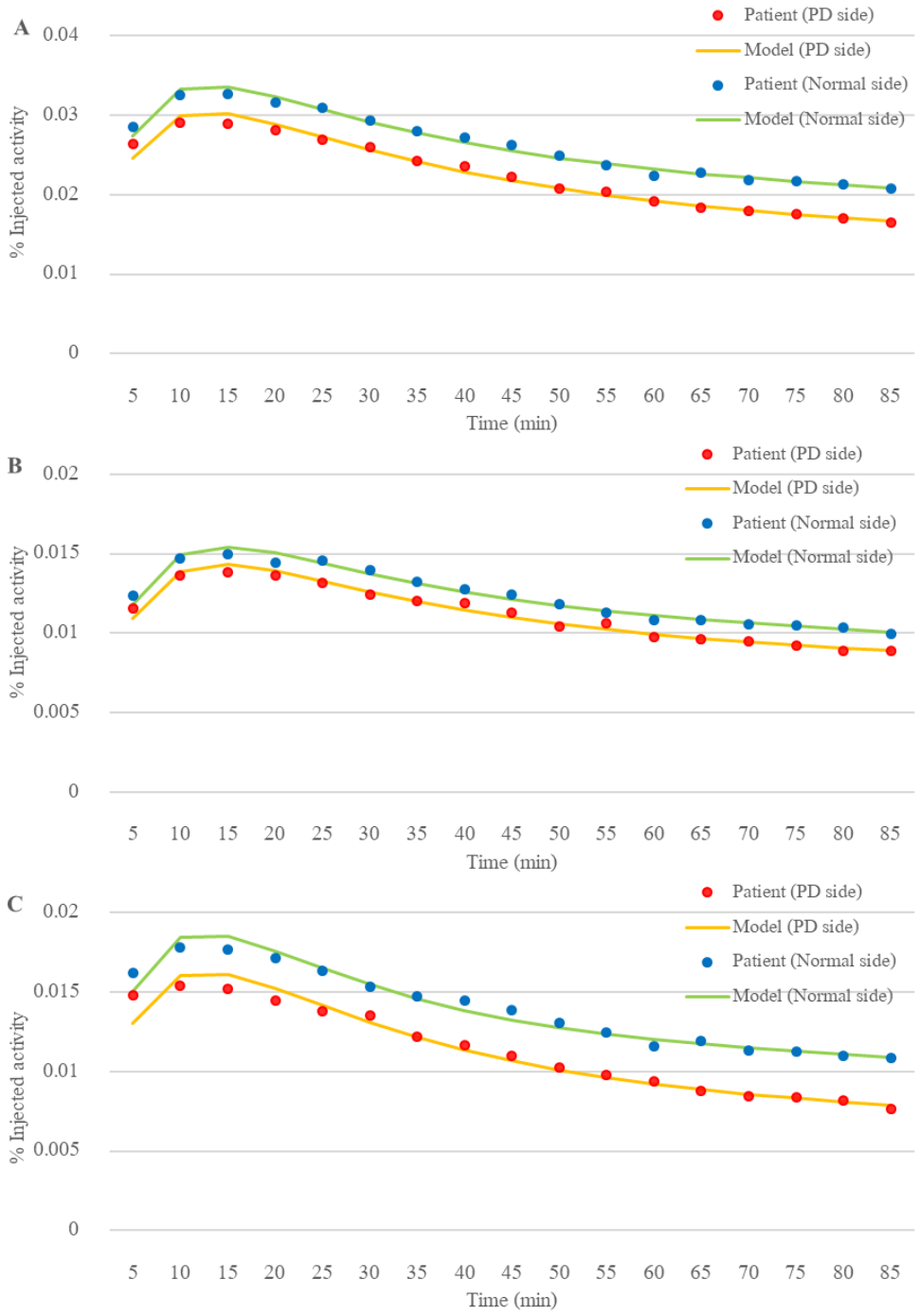

Figure 38 The Patient no 4's time-activity curves in the striatum (A), caudate (B) and putamen (C).

* Blue and red round markers represent patient's data obtained from contralateral and ipsilateral side respectively. Green and yellow lines represent the model fitted from contralateral and ipsilateral side respectively.

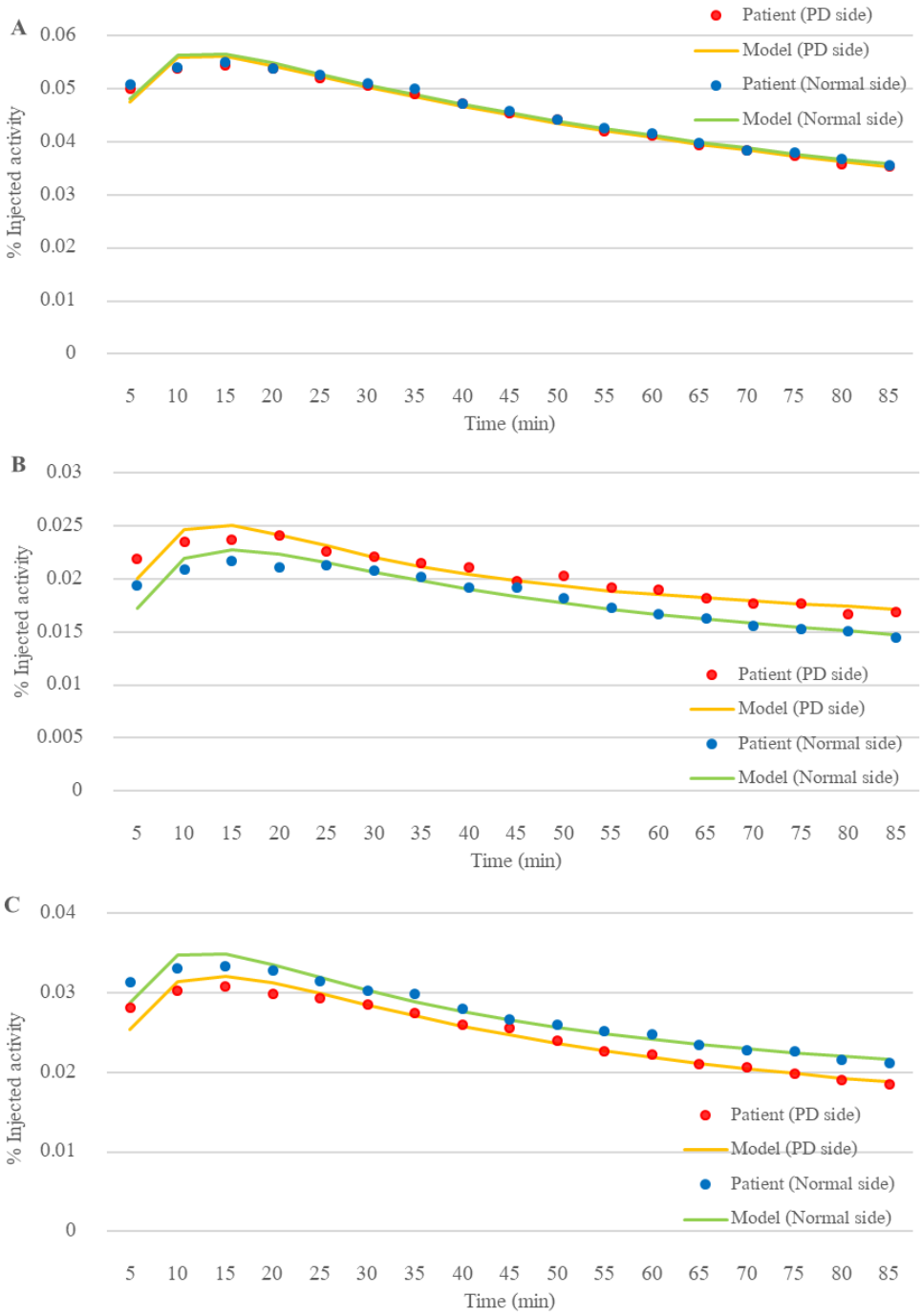

Figure 39 The Patient no 5's time-activity curves in the striatum (A), caudate (B) and putamen (C).

* Blue and red round markers represent patient's data obtained from contralateral and ipsilateral side respectively. Green and yellow lines represent the model fitted from contralateral and ipsilateral side respectively.

Figure 40 depicts the mean time-activity curves obtained in both ipsilateral and contralateral side after ^{18}F-FDOPA injection in striatum (Figure 40A), caudate (Figure 40B) and putamen (Figure 40C). The measured FDOPA curves were fitted well by a three-compartment, three-rate constant model with mean AIC -5.72 and BIC -5.62 (Table 13) Both curves increased at the initial of the model until reached the maximum uptake activity at 15-min time point then slightly decreased accordingly. The contralateral side of striatum (Figure 40A) had lower uptake than the ipsilateral side. Likewise, the tendency of the biokinetic of putamen time-activity curves (Figure 40C) has clearer difference of the curve fitting model between contralateral and ipsilateral side of putamen. However, the caudate time-activity curves nearly superimposed to each other as in Figure 40B.

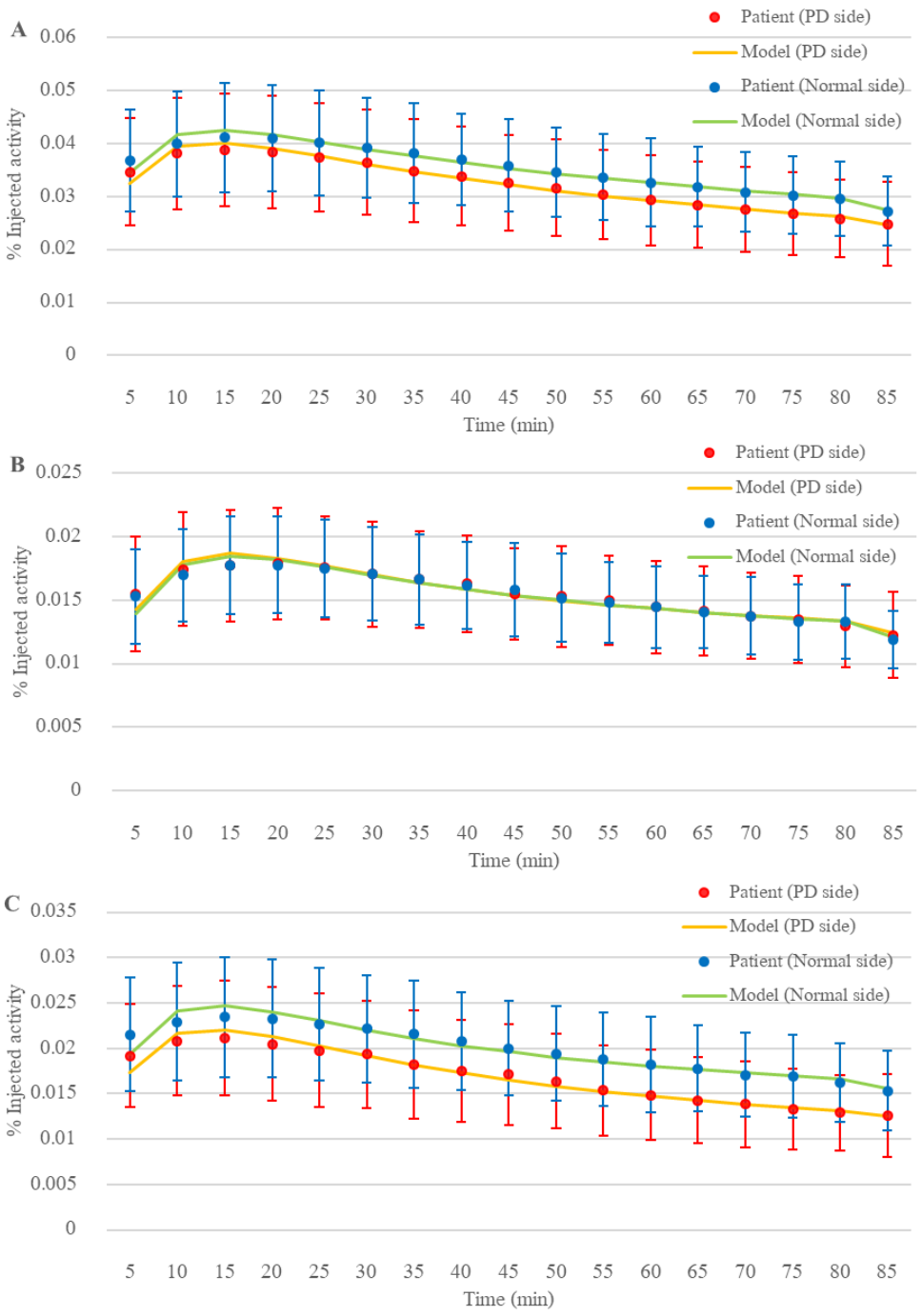

Figure 40 The mean time-activity curves in the striatum (A), caudate (B) and putamen (C).

* Blue and red round markers represent patient's data obtained from contralateral and ipsilateral side respectively. Green and yellow lines represent the model fitted from contralateral and ipsilateral side respectively.

Table 10 and Figure 41 depict the transfer rate constants for both side of striatum. In contralateral striatum, K_1 was 0.0231 ml min^{-1} g^{-1}; k_2 was 0.0196 min^{-1}; and k_3 was 0.0112 min^{-1} while the ipsilateral, K_1 was 0.0245 ml min^{-1} g^{-1}; k_2 was 0.0178 min^{-1}; and k_3 was 0.0152 min^{-1}. According to the statistical analysis based on Wilcoxson signed rank test for non-parametric variables, we found that there were statistically significant differences between contralateral and ipsilateral side of striatum in K_1 and k_3 (p-value < 0.05).

Table 11 and Figure 42 depict the results in caudate region. For the contralateral caudate, K_1 was 0.0094 ml min^{-1} g^{-1}; k_2 was 0.0237 min^{-1}; and k_3 was 0.0203 min^{-1} while the ipsilateral, K_1 was 0.0091 ml min^{-1} g^{-1}; k_2 was 0.0228 min^{-1}; and k_3 was 0.0215 min^{-1}. There were insignificant differences between both sides of caudate.

The results of transfer rate constants in putamen are shown as in Table 12 and Figure 43. In the contralateral putamen, K_1 was 0.0116 ml min^{-1} g^{-1}; k_2 was 0.0268 min^{-1}; and k_3 was 0.0112 min^{-1}, while the ipsilateral, K_1 was 0.0131 ml min^{-1} g^{-1}; k_2 was 0.0254 min^{-1}; and k_3 was 0.0176 min^{-1}. We found that there were statistically significant differences between contralateral and ipsilateral side of putamen in K_1 and k_3 (p-value < 0.05).

Table 10 Transfer rates of striatum.

Patient	Contralateral striatum			Ipsilateral striatum		
	K_1 (ml/min/g)	k_2 (/min)	k_3 (/min)	K_1 (ml/min/g)	k_2 (/min)	k_3 (/min)
1	0.0221 (0.0005)	0.0155 (0.0034)	0.0064 (0.0049)	0.0242 (0.0008)	0.0159 (0.0051)	0.0111 (0.0091)
2	0.0254 (0.0005)	0.0203 (0.002)	0.0165 (0.0028)	0.0268 (0.0007)	0.0125 (0.0028)	0.0210 (0.0041)
3	0.0357 (0.0008)	0.0163 (0.0035)	0.0079 (0.0045)	0.0363 (0.0009)	0.0168 (0.0041)	0.0088 (0.0102)
4	0.0170 (0.0005)	0.0287 (0.0026)	0.0105 (0.0017)	0.0192 (0.0005)	0.0283 (0.0025)	0.0159 (0.002)
5	0.0154 (0.0009)	0.0171 (0.0021)	0.0146 (0.0029)	0.0160 (0.001)	0.0154 (0.0023)	0.0195 (0.0031)
Mean (SD)	0.0231 (0.0081)	0.0196 (0.0054)	0.0112 (0.0043)	0.0245 (0.0078)	0.0178 (0.0061)	0.0152 (0.0053)

Table 11 Transfer rates of caudate.

Patient	Contralateral caudate			Ipsilateral caudate		
	K_1 (ml/min/g)	k_2 (/min)	k_3 (/min)	K_1 (ml/min/g)	k_2 (/min)	k_3 (/min)
1	0.0095 (0.0002)	0.0214 (0.0039)	0.0129 (0.0083)	0.0095 (0.0003)	0.0228 (0.0065)	0.0163 (0.01)
2	0.0104 (0.0003)	0.0258 (0.0034)	0.0315 (0.0036)	0.0109 (0.0003)	0.0251 (0.0036)	0.0352 (0.0036)
3	0.0137 (0.0005)	0.0317 (0.0066)	0.0246 (0.0081)	0.0113 (0.0005)	0.0201 (0.0070)	0.0121 (0.0094)
4	0.0071 (0.0002)	0.0265 (0.0026)	0.0144 (0.0021)	0.0077 (0.0002)	0.0264 (0.0024)	0.0171 (0.0021)
5	0.0061 (0.0006)	0.0130 (0.0056)	0.0183 (0.0045)	0.0061 (0.0005)	0.0193 (0.0038)	0.027 (0.0042)
Mean (SD)	0.0094 (0.0030)	0.0237 (0.007)	0.0203 (0.0077)	0.0091 (0.0022)	0.0228 (0.0031)	0.0215 (0.0094)

Table 12 Transfer rates of putamen.

Patient	Contralateral putamen			Ipsilateral putamen		
	K_1 (ml/mi/g)	k_2 (/min)	k_3 (/min)	K_1 (ml/min/g)	k_2 (/min)	k_3 (/min)
1	0.0109 (0.0004)	0.0209 (0.0053)	0.0098 (0.0041)	0.0124 (0.0090)	0.0211 (0.0204)	0.0146 (0.0191)
2	0.0128 (0.0003)	0.0301 (0.0026)	0.0148 (0.0026)	0.0136 (0.0005)	0.0203 (0.0044)	0.0208 (0.0048)
3	0.0173 (0.0005)	0.0214 (0.0042)	0.0081 (0.0031)	0.0202 (0.0006)	0.0286 (0.0051)	0.0161 (0.0069)
4	0.0087 (0.0004)	0.0344 (0.0039)	0.0094 (0.0019)	0.0102 (0.0004)	0.0366 (0.0040)	0.0174 (0.0023)
5	0.0084 (0.0006)	0.0272 (0.0030)	0.0142 (0.0028)	0.0090 (0.0008)	0.0204 (0.0040)	0.0191 (0.0031)
Mean (SD)	0.0116 (0.0037)	0.0268 (0.0057)	0.0112 (0.003)	0.0131 (0.0044)	0.0254 (0.0072)	0.0176 (0.0025)

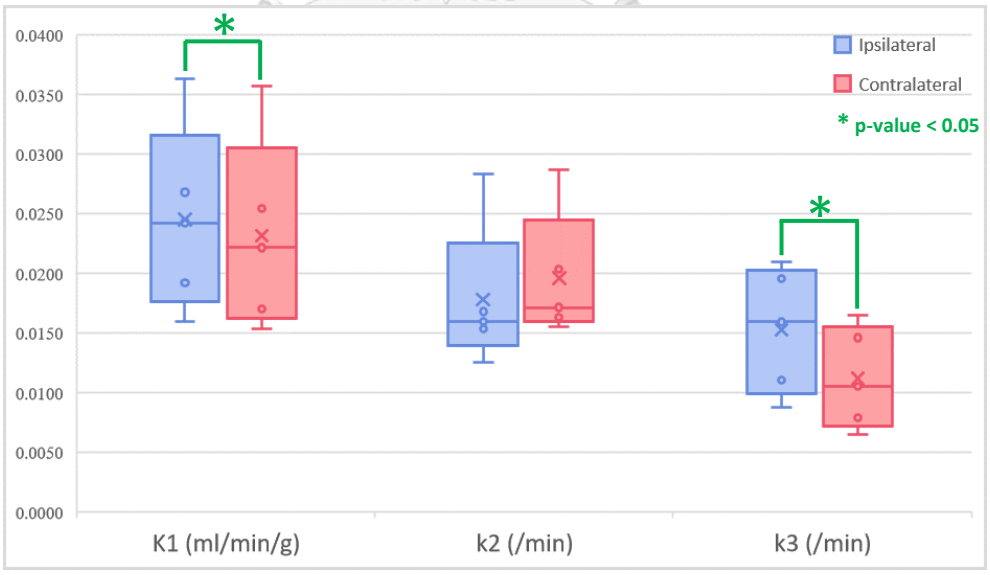

Figure 41 Box plots of transfer rate constants in contralateral (red) and ipsilateral (blue) striatum.

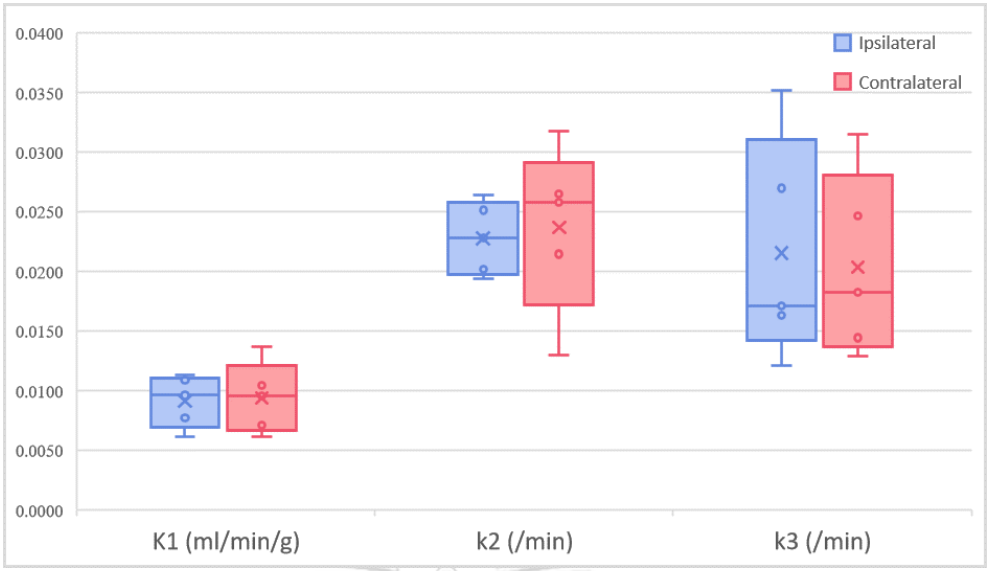

Figure 42 Box plots of transfer rate constants in contralateral (red) and ipsilateral (blue) caudate.

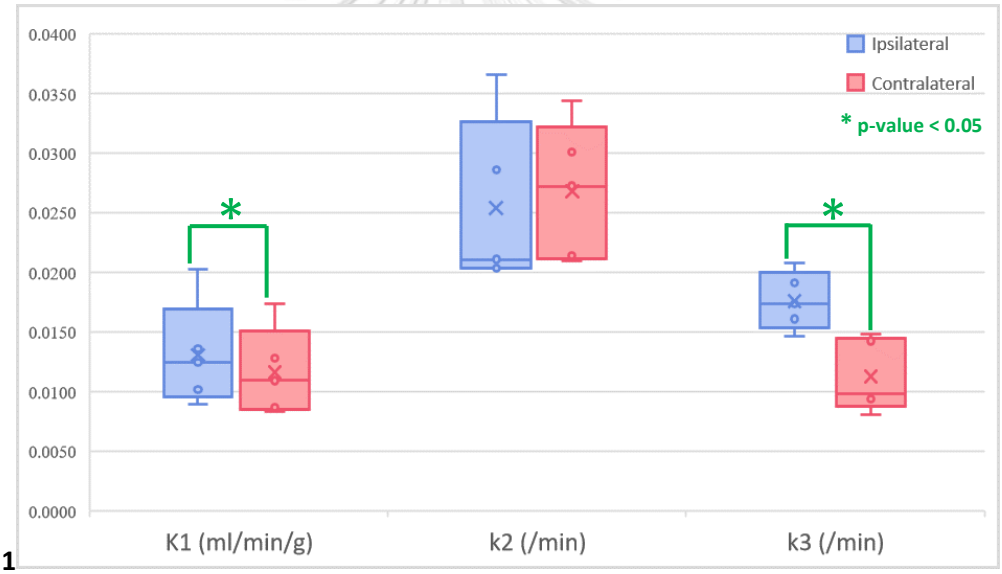

1

Figure 43 Box plots of transfer rate constants in contralateral (red) and ipsilateral (blue) putamen.

Table 13 AIC and BIC of the model in each region.

Region	AIC	BIC
Striatum		
Contralateral	-5.55	-5.45
Ipsilateral	-5.41	-5.31
Mean	-5.48	-5.38
Caudate		
Contralateral	-5.98	-5.88
Ipsilateral	-5.97	-5.87
Mean	-5.98	-5.88
Putamen		
Contralateral	-5.79	-5.69
Ipsilateral	-5.6	-5.5
Mean	-5.7	-5.6
Total Mean	-5.72	-5.62

CHAPTER 5

DISCUSSION AND CONCLUSIONS

5.1 Discussion

Parkinson's disease PET diagnosis has been mostly interpreting the images by qualitative examination, but misinterpretation may occur due to the observers' experiences. Therefore, many specific methods of quantification analysis have been proposed. Compartmental model is one of the pharmacokinetic quantitative analysis approaches that widely used to simulate physiologically significant parameters.

In 1991, Huang SC, et al[22] suggested the pharmacokinetic model consisting of three separated compartments for tissue FDOPA, FDA and its metabolites, and tissue OMFD with 6 transfer rate constants could describe adequately the striatal kinetics in humans. The transfer rate constants were measured in 10 normal human subjects with PET brain scan from 0 to 120 min after an intravenous bolus injection of the ^{18}F-FDOPA tracer. The arterial plasma concentrations of the tracer and its metabolites were defined by biochemical assay and used as input function to the model.

Later on, the kinetic parameters of ^{18}F-FDOPA in striatum were measured with PET from 0 to 150 min after an intravenous bolus injection of tracer in four normal subjects and two patients suffering from Parkinson's disease by Wahl L and Nahmias C[24]. On a separate occasion, the kinetic parameters of OMFD were determined in the plasma and striatum of the same individuals. They found that the forward transport rates for ^{18}F-FDOPA and OMFD from plasma to striatal tissue are very similar in humans, therefore the number of compartments and rate constants of striatal pharmacokinetics could reduce into two tissue compartments for tissue FDOPA, tissue FDA and its metabolites, and three transfer rate constants. The difference of transfer rate constants between normal subjects and PD patients was found in k_3, although the stages of PD patients hadn't been considered in this research studies.

In the present study, we investigated the transfer rate constants of ^{18}F-FDOPA in PET brain imaging based on compartmental model in early Parkinson's disease and then classified the difference between both sides of striatum including caudate and putamen. Our compartmental model has modified in accordance with Wahl and Nahmias's study. With image-based analysis, the percentages of injected activity in each time point were used as an input function. Although one of our patients lost the last time point data at 85-minute, there was no influence on time-activity curve simulation fitting.

The between-side analysis showed that the mean transfer rate constants values of K_1 and k_3 in the contralateral (PD side) striatum and putamen were significantly lesser than those in the ipsilateral (normal side) with p-value < 0.05, and was more pronounced in the putamen while the statistically insignificant difference was found in the caudate transfer rate constants values. This finding is corresponding with the results of the PD imaging studies, which suggested that the dopamine depletion began in the posterior parts of the putamen and proceeded during the disease to the caudate nucleus and other parts of the dopaminergic system. The decrease in ^{18}F-FDOPA uptake in the present study was larger in the contralateral striatum, because motor symptoms have been shown to be more severe on the side contralateral to the striatum with lower dopaminergic activity[5]. However, our outcome may represent the majority in patient with stage two of PD who had right side predominant symptoms or lose activity uptake in left striatum even though random sample collection was performed.

Instead of providing the transfer rate constants only in striatum as an extension of the previous study[22, 24], our findings also determined transfer rate constants in caudate and putamen. This could be help to deeply specific in biokinetics of the pathologic region. The comparison of transfer rate constant and patient data collection method between literatures review and present study are shown in Table 14 and Figure 44-45.

Table 14 The comparison of transfer rate constant between literatures review and this study.

Study	**Huang et al. (JCBFM 1991)**	**Wahl & Nahmias (JNM 1996)**	**This study**
Overall Demographic			
Subjects	Normal = 10	Normal = 4, PD = 2	PD = 5
Hoehn and Yahr Stage	N/A	Late	Early
PET scan (min)	120	150	90
Patient data collection method	Blood sampling and image analysis	Blood sampling and image analysis	Image-based analysis
The Average (SD) of Transfer Rate Constants in Ipsilateral Striatum (Normal)			
K_1 (ml/min/g)	0.0283 (0.0051)	0.0403 (0.0177)	0.0245 (0.0078)
k_2 (/min)	0.0228 (0.0048)	0.0342 (0.0185)	0.0178 (0.0061)
k_3 (/min)	0.0124 (0.0041)	0.0124 (0.0058)	0.0152 (0.0053)
The Average (SD) of Transfer Rate Constants in Contralateral Striatum (PD)			
K_1 (ml/min/g)		0.0494 (0.0072)	0.0231 (0.0081)
k_2 (/min)	N/A	0.0281 (0.0072)	0.0196 (0.0054)
k_3 (/min)		0.0043 (0.001)	0.0112 (0.0043)

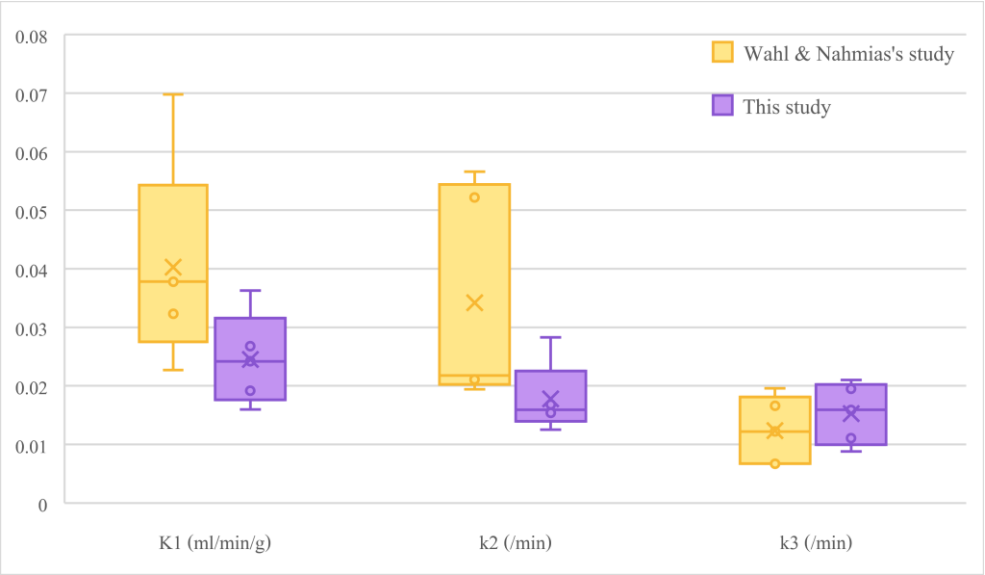

Figure 44 Box plots of transfer rate constants in ipsilateral striatum (normal) compared between literatures review and this study.

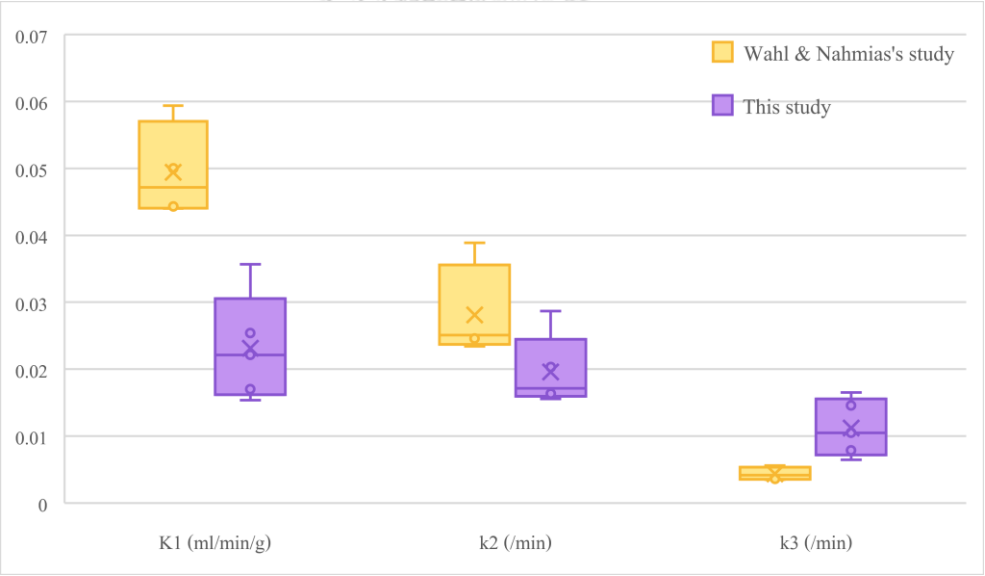

Figure 45 Box plots of transfer rate constants in contralateral striatum (PD) compared between literatures review and this study.

The striatal transfer rate constants for K_1 and k_2 of both sides in our study was approximately 2-fold lower than Wahl & Nahmias's study but comparable to Huang's study. The patients' characteristic is assumed to be the cause of the difference in transfer rate constant. However, the variation according to Wahl & Nahmias was quite high competed to ours and Huang's study.

In contrast, the striatal transfer rate constant k_3 in PD patients in our study was 2.6-fold higher than Wahl and Nahmias's study. One factor that may explain this is the difference in disease's severity. As our study was conducted in early PD patients with distinct inclusion criteria following HY score limited to 2, the loss of dopaminergic neurons in our patients may lesser than their study. Even though the clinical rating scale of the patients had not been mentioned in Wahl and Nahmias's study, their results implicitly indicated that patients may suffer from late stages of PD.

Our evidences suggested that K_1 and k_3 are the parameters to differentiate between PD and normal patients, whereas Wahl and Nahmias's study found only in k_3. It was possibly due to the difference in patient data collection method. The simulation of our patient data was image-based analysis acquired from radioactivity uptake in brain region, while the study from Wahl and Nahmias or Huang et al collected patient data by the combination of arterialized venous blood sampling and image analysis. The biochemical assay method could be more preferable for pharmacokinetic modeling, but with the image-based analysis could be more practical, less invasive, reduce occupational dose, and able to work with retrospective data.

The limitations of this study were; firstly, the transfer rate constants were compared between sides instead of the comparison between normal subjects and PD patients. In our study, the contralateral side of patient's striatum, caudate or putamen that had lower radioactivity uptake was considered as PD and the another as normal according to the progression of the disease. Therefore, the patient data of ipsilateral side might not be truly normal as expected. Secondly, The PET template used for co-registration and normalization in SPM software was implicitly derived from ^{15}Oxygen labelled water and spatially normalized to International Consortium for Brain Mapping (ICBM). Additionally, the striatum, caudate and putamen template were created from the AAL-VOIs atlas resulting from T1 MRI data set provided by the Montreal Neurological Institute (MNI). Ideally, automated segmentation using SPM in striatum, caudate and putamen should be based on the patient's MRI individual for the best localization. However, PET brain scan along with MRI scan hasn't established as a routine protocol at KCMH yet. Additionally, patients' CT images couldn't provide enough sub-regions anatomical structure in striatum as MRI. Therefore, segmented regions in every patient had the same volume and may not give perfect co-registration and segmentation accordingly. These could be a source of uncertainty for the ^{18}F-FDOPA quantification in brain tissue for generating the time-activity curve to simulate the kinetic model.

As the sample size of this study was relatively small, the generalization of our finding could be limited. Therefore, it is recommended that the further studies with a larger sample size should be conducted.

5.2 Conclusions

Parkinson's disease is the second most common neurodegenerative disorder which tend to rise up to almost 15% in Thai population. However, there has been a lack of information on the quantitative parameters in ^{18}F-FDOPA PET studies obtained in Thai PD patients. This study, therefore, aimed to explore the transfer rate constants of ^{18}F-FDOPA in Thai early Parkinson's disease based on compartmental model. The two-tissue compartmental and three-transfer rate constants model was able to describe ^{18}F-FDOPA kinetics in striatum, caudate and putamen similar to previous studies. In accordance with our finding, we can conclude that both K_1 and k_3 from striatum and putamen on contralateral side to patient's symptom are likely to be the predictor quantitative parameters for diagnosis of early PD. However, the biokinetic data from healthy subjects are needed for the result confirmation. The pharmacokinetic model of ^{18}F-FDOPA according to this study may be used as an initial reference report for Parkinson's disease in Thai patients.

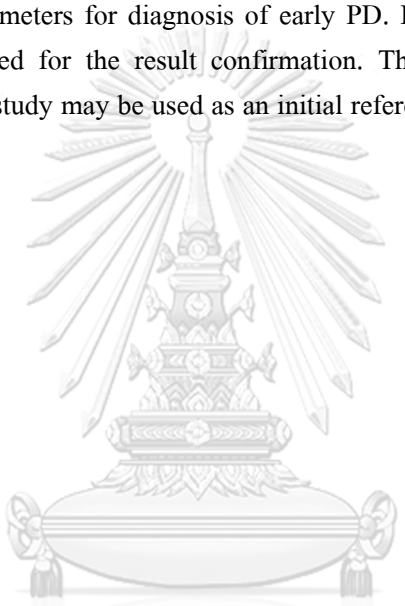

REFERENCES

1. David G. Standaert MHS-H, Cathi A. Thomas. Parkinson's Disease Handbook: American Parkinson Disease Association (APDA).

2. Brooks DJ. Neuroimaging in Parkinson's disease. NeuroRx. 2004;1(2):243-54.

3. DeMaagd G, Philip A. Parkinson's disease and its management: part 1: disease entity, risk factors, pathophysiology, clinical presentation, and diagnosis. Pharmacy and therapeutics. 2015;40(8):504.

4. Anti$\acute{C}$ S, Lisak M, Trkanjec Z, Demarin V. Parkinsonova bolest. Acta Clin Croat. 2009;48:377-80.

5. Lang AE, Lozano AM. Parkinson's disease. New England Journal of Medicine. 1998;339(16):1130-43.

6. Bhidayasiri R, Tarsy D. Parkinson's disease: hoehn and yahr scale. Movement Disorders: A Video Atlas: Springer; 2012. p. 4-5.

7. Shukla AK, Kumar U. Positron emission tomography: An overview. J Med Phys. 2006;31(1):13-21.

8. Badawi R. Introduction to PET Physics 1999 [Available from: https://depts.washington.edu/nucmed/IRL/pet_intro/toc.html.

9. Saha GB. Basics of PET imaging: physics, chemistry, and regulations: Springer; 2015.

10. Seo Y, Teo BK, Hadi M, Schreck C, Bacharach SL, Hasegawa BH. Quantitative accuracy of PET/CT for image-based kinetic analysis. Med Phys. 2008;35(7):3086-9.

11. Fahey FH. Data acquisition in PET imaging. Journal of nuclear medicine technology. 2002;30(2):39-49.

12. Leung K. L-3, 4-Dihydroxy-6-[18F] fluorophenylalanine. Molecular Imaging and Contrast Agent Database (MICAD)[Internet]: National Center for Biotechnology Information (US); 2011.

13. Loane C, Politis M. Positron emission tomography neuroimaging in Parkinson's disease. Am J Transl Res. 2011;3(4):323-41.

14. Morris ED, Endres CJ, Schmidt KC, Christian BT, Muzic RF, Fisher RE. Kinetic modeling in positron emission tomography. Emission Tomography: The Fundamentals of PET and SPECT Academic, San Diego. 2004.

15. Watabe H, Ikoma Y, Kimura Y, Naganawa M, Shidahara M. PET kinetic analysis--compartmental model. Ann Nucl Med. 2006;20(9):583-8.

16. Vicini P, Brill AB, Stabin MG, Rescigno A. Kinetic modeling in support of radionuclide dose assessment. Semin Nucl Med. 2008;38(5):335-46.

17. Nelissen N, Dupont P. Kinetic modelling in human brain imaging. Positron Emission Tomography-Current Clinical and Research Aspects: IntechOpen; 2012.

18. Stephanie. Akaike's Information Criterion: Definition, Formulas 2015 [Available from: https://www.statisticshowto.datasciencecentral.com/akaikes-information-criterion/.

19. Bozdogan H. Model selection and Akaike's information criterion (AIC): The general theory and its analytical extensions. Psychometrika. 1987;52(3):345-70.

20. Stephanie. Bayesian Information Criterion (BIC) / Schwarz Criterion 2018 [Available from: https://www.statisticshowto.datasciencecentral.com/bayesian-information-criterion/.

21. Schwarz G. Estimating the Dimension of a Model. The Annals of Statistics. 1978;6(2):461-4.

22. Huang SC, Yu DC, Barrio JR, Grafton S, Melega WP, Hoffman JM, et al. Kinetics and modeling of L-6-[18F]fluoro-dopa in human positron emission tomographic studies. J Cereb Blood Flow Metab. 1991;11(6):898-913.

23. Kuwabara H, Cumming P, Reith J, Leger G, Diksic M, Evans AC, et al. Human striatal L-dopa decarboxylase activity estimated in vivo using 6-[18F]fluoro-dopa and positron emission tomography: error analysis and application to normal subjects. J Cereb Blood Flow Metab. 1993;13(1):43-56.

24. Wahl L, Nahmias C. Modeling of fluorine-18-6-fluoro-L-Dopa in humans. J Nucl Med. 1996;37(3):432-7.

25. Hughes A, Ben-Shlomo Y, Daniel S, Lees A. UK Parkinson's disease society brain bank clinical diagnostic criteria. J Neurol Neurosurg Psychiatr. 1992;55(181):e4.

26. William Penny KF, John Ashburner, Stefan Kiebel, Thomas Nichols. Statistical Parametric Mapping: The Analysis of Functional Brain Images. 1st ed2006.

27. Schneider CA, Rasband WS, Eliceiri KW. NIH Image to ImageJ: 25 years of image analysis. Nature Methods. 2012;9(7):671-5.

28. SAAM II Version 2.1: University of Washington and The Epsilon Group; 2011.

29. IAEA. QUALITY ASSURANCE FOR PET AND PET/CT SYSTEMS2009.

APPENDICES

APPENDIX A

Report of PET/CT System Quality Control

Location: 2nd floor, Division of Nuclear Medicine, Bhumisiri Mangkhalanusorn Building, King Chulalongkorn Memorial Hospital

Date: 17 January 2019

Manufacturer: Siemens Medical Solutions

Model: Biograph 16 PET/CT HI-REZ system

Image quality

Objective: to evaluate the images quality of the PET system by simulating a whole-body imaging study with both hot and cold lesions.

Methods:

The image quality control of PET/CT system was performed according to NEMA NU2-2007 protocol[29] using an International Electric Commission (IEC) body phantom. The phantom consists of a body phantom, a lung-insert and an insert with six fillable spheres with 10, 13, 17, 22, 28 and 37 mm inner diameter. Unfortunately, 10, 13 and 37 mm diameter spheres in our phantom were obstructed and unable to fill the solution. As a result, the smallest sphere of 10 mm diameter was excluded from data analysis.

The warm background within the body compartment of the phantom was first filled with ^{18}F solution activity concentration of 5.3 kBq/cc. The 17 and 22 mm diameter spheres were sequentially filled with activity concentrations of 8 and 4 times of the background and considered as hot spheres. The 28 mm diameter sphere was then filled with non-radioactive water and considered as cold sphere as well as 13 and 37 mm inner diameter. To simulate the radioactivity outside the scanner FOV, the polyethylene cylindrical line source of the 70-cm scatter phantom was filled with 120.99 MBq (3.27 mCi) of ^{18}F solution to yield an effective activity concentration equal to the background activity concentration used in the IEC body phantom. Such line source was placed together at the lower edge of the body phantom as shown in Figure 46.

Figure 46 Positioning of IEC body phantom and scatter phantom for testing image quality of PET/CT system.

The acquisition protocol was set as a routine whole-body protocol. Ordered subset expectation maximization (OSEM) iterative algorithm with 4 iterations and 8 subsets, matrix size of 168 x 168, slice thickness of 4 mm was used for image reconstruction.

Analysis:

The percent contrast for both hot and cold spheres were then analyzed. The residual error in the lung region were also reported. In order to determine the contrast in transverse image, the circular ROIs were drawn in both hot and cold lesions according to the inner diameter in each sphere. Twelve 37 mm diameter circular ROIs were also drawn throughout the background at a distance of 1.5 cm from the edge of the phantom (Figure 47).

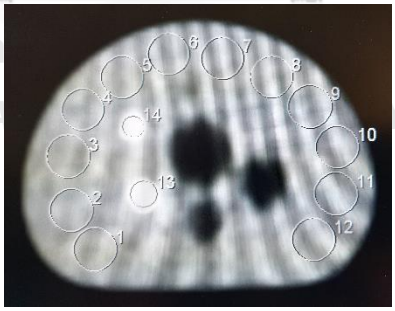

Figure 47 Example of ROIs placement on IEC body phantom image for quantitative analysis.

The percent contrast (Q_H) in hot sphere can be calculated as followings:

$$Q_H = \frac{\left(C_{hot} - C_{bg}\right)/C_{bg}}{\left(a_{hot} - a_{bg}\right)/a_{bg}} \times 100$$

where C_{hot} is the average counts in the ROI for each hot sphere, C_{bg} is the average of the twelve background ROI counts, a_{hot} is the radioactivity concentration in the hot spheres and a_{bg} is the activity concentration in the background.

The percent contrast in cold sphere (Q_C) can be then computed as:

$$Q_C = \frac{\left(C_{bg} - C_{cold}\right)}{C_{bg}} \times 100$$

where C_{cold} is the average of the counts in the ROI for each cold sphere.

To measure the residual error in scatter and attenuation corrections, the relative error (ΔC_{lung}) in percentage unit for each slice can be calculated as:

$$\Delta C_{lung} = \frac{C_{lung}}{C_{bg}} \times 100$$

where C_{lung} is the average counts in the ROI placed over the lung insert.

Results:

Table 15 Percent contrast and lung residual error with source-to-background ratio 4:1.

Sphere diameter (mm)	Contrast (%)
13	39.85
17	54.49
22	60.52
28	64.45
37	67.27
the relative error (%)	24.63

Table 16 Percent contrast and lung residual error with source-to-background ratio 8:1.

Sphere diameter (mm)	Contrast (%)
13	41.5
17	55.51
22	61.56
28	69.22
37	70.61
the relative error (%)	19.54

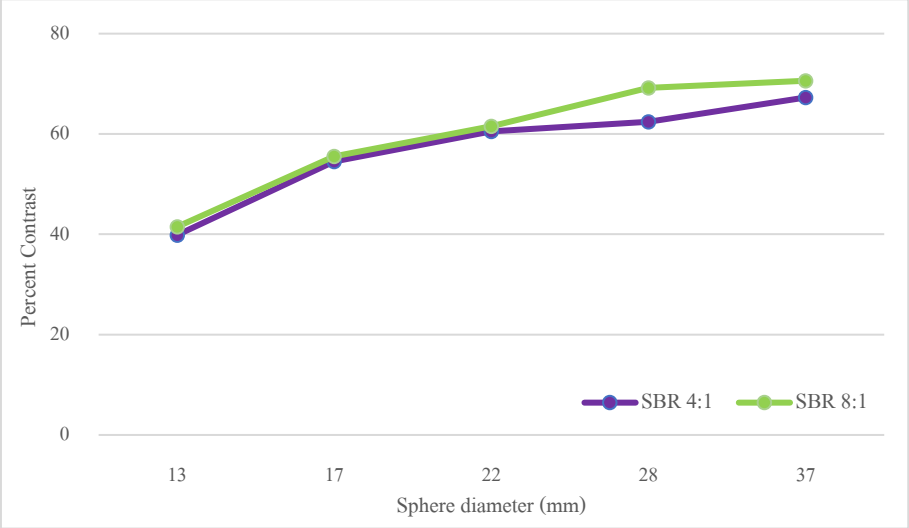

Figure 48 Percent contrast with source-to-background ratio 4:1 and 8:1.

The percent contrast of hot and cold spheres ranged of 39.85 - 67.27 was seen at source-to-background ratio (SBR) 4, while 41.5 - 70.61 was observed at SBR 8. Both SBRs were reconstructed with the parameters used as clinical study (OSEM, 4 iterations and 8 subsets). The relative error in lung region were 24.63 (SBR 4) and 19.54 (SBR 8) respectively. As expected, at SBR 8 provides the percent contrast slightly better than SBR 4. The percent contrast was increased with increasing sphere diameter at both SBRs.

Based on the IAEA human health series no.1 recommendation[29], the tolerance criterion should be within 5% compared to the baseline established values for all image quality parameters. According to the results, the image quality was still within the tolerance of the latest testing in 2010.

APPENDIX B

The Approval of Institutional Review Board

Certificate of research approval from Institutional Review Board (IRB) of Faculty of Medicine, Chulalongkorn University, Bangkok, Thailand.

COA No. 774/2018
IRB No. 361/61

INSTITUTIONAL REVIEW BOARD
Faculty of Medicine, Chulalongkorn University
1873 Rama 4 Road, Patumwan, Bangkok 10330, Thailand, Tel 662-256-4493

Certificate of Approval

The Institutional Review Board of the Faculty of Medicine, Chulalongkorn University, Bangkok, Thailand, has approved the following study which is to be carried out in compliance with the International guidelines for human research protection as Declaration of Helsinki, The Belmont Report, CIOMS Guideline and International Conference on Harmonization in Good Clinical Practice (ICH-GCP)

Study Title : The pharmacokinetic model of ^{18}F-FDOPA in PET brain imaging for early Parkinson's disease.

Study Code : -

Principal Investigator : Miss Wirunpatch Buratachwatanasiri

Affiliation of PI : Department of Radiology,
Faculty of Medicine, Chulalongkorn University.

Review Method : Expedited

Continuing Report : At least once annually or submit the final report if finished.

Document Reviewed :

1. Research Proposal Version 2.0 Date Aug 9, 2018
2. Protocol Synopsis Version 2.0 Date Aug 9, 2018
3. CASE RECORD FORM Version 2.0 Date Aug 9, 2018
4. Curriculum Vitae and GCP Training
   - Miss Wirunpatch Buratachwatanasiri
   - Kitiwat Khamwan, Ph.D.

Signature .....
(Emeritus Professor Tada Sueblinvong MD)
Chairperson
The Institutional Review Board

Signature .....
(Associate Professor Supeecha Wittayalertpanya)
Member and Assistant Secretary, Acting Secretary
The Institutional Review Board

Date of Approval : August 14, 2018
Approval Expire Date : August 13, 2019

Approval granted is subject to the following conditions: (see back of this Certificate)

APPENDIX C

Case Record Form

PATIENT NUMBER _____

Patient's Demographic			
Patient number			
Age (Years)			
Gender	☐ Male	☐ Female	
Clinical Symptom	☐ Bradykinesia	☐ Resting tremor	☐ Rigidity
Predominant Symptom	☐ Right	☐ Left	
HY Scale			
Date of PET Study	__ __ / __ __ / __ __ __ __		
Injected Activity (MBq)			
Decreased Activity Uptake Side	☐ Right	☐ Left	

Scaling Factor Calculation						
Time point	**Image**	**Count**	**Mean**	**Voxel value (Bq/ml)**	**Voxel value (Bq)**	**Scaling factor**
5	Original					
	Normalized					
10	Original					
	Normalized					
15	Original					
	Normalized					
20	Original					
	Normalized					
25	Original					

	Normalized					
30	Original					
	Normalized					
35	Original					
	Normalized					
40	Original					
	Normalized					
45	Original					
	Normalized					
50	Original					
	Normalized					
55	Original					
	Normalized					
60	Original					
	Normalized					
65	Original					
	Normalized					
70	Original					
	Normalized					
75	Original					
	Normalized					
80	Original					
	Normalized					
85	Original					
	Normalized					
Mean Scaling Factor						

% Injected Activity Calculation of Right Striatum					
Time point	**Count**	**Mean**	**Voxel value**	**Activity (MBq)**	**% Injected activity**
5					
10					
15					
20					
25					
30					
35					
40					
45					
50					
55					
60					
65					
70					
75					
80					
85					

% Injected Activity Calculation of Left Striatum					
Time point	**Count**	**Mean**	**Voxel value**	**Activity (MBq)**	**% Injected activity**
5					
10					
15					
20					
25					
30					
35					
40					
45					
50					
55					
60					
65					
70					
75					
80					
85					

% Injected Activity Calculation of Right Caudate					
Time point	**Count**	**Mean**	**Voxel value**	**Activity (MBq)**	**% Injected activity**
5					
10					
15					
20					
25					
30					
35					
40					
45					
50					
55					
60					
65					
70					
75					
80					
85					

% Injected Activity Calculation of Left Caudate					
Time point	**Count**	**Mean**	**Voxel value**	**Activity (MBq)**	**% Injected activity**
5					
10					
15					
20					
25					
30					
35					
40					
45					
50					
55					
60					
65					
70					
75					
80					
85					

% Injected Activity Calculation of Right Putamen					
Time point	**Count**	**Mean**	**Voxel value**	**Activity (MBq)**	**% Injected activity**
5					
10					
15					
20					
25					
30					
35					
40					
45					
50					
55					
60					
65					
70					
75					
80					
85					

% Injected Activity Calculation of Left Putamen					
Time point	**Count**	**Mean**	**Voxel value**	**Activity (MBq)**	**% Injected activity**
5					
10					
15					
20					
25					
30					
35					
40					
45					
50					
55					
60					
65					
70					
75					
80					
85					

Simulated Time Activity Curve						
Time point	**Striatum**		**Caudate**		**Putamen**	
	Right	**Left**	**Right**	**Left**	**Right**	**Left**
5						
10						
15						
20						
25						
30						
35						
40						
45						
50						
55						
60						
65						
70						
75						
80						
85						

Transfer Rate Constants				
Region		**K_1**	**k_2**	**k_3**
Striatum	Right			
	Left			
Caudate	Right			
	Left			
Putamen	Right			
	Left			

AIC: _____

BIC: _____

VITA

NAME	Wirunpatch Buratachwatanasiri
DATE OF BIRTH	6 October 1992
PLACE OF BIRTH	Bangkok
INSTITUTIONS ATTENDED	- Master of Medical Imaging, Chulalongkorn University - Bachelor of Science (Radiological Technology), Mahidol University
HOME ADDRESS	59/2 Sukumvit 49/4 Road, Khwaeng Khlong Tan Nuea, Khet Watthana, Krung Thep Maha Nakhon 10110, Thailand
PUBLICATION	Buratachwatanasiri W., Chantadisai M., Khamwan K. Pharmacokinetic modeling of 18F-FDOPA PET in human brain for early Parkinson's disease. In Proceeding of 11th Annual Scientific Meeting of Thai Medical Physicist Society (TMPS), pp 93-96, Chonburi, Thailand, 2019
AWARD RECEIVED	- Excellent Presentation in Nuclear Medicine from the 11th Thai Medical Physicist Society (TMPS), Thailand - Best Oral Presentation from the 18th Asia-Oceania Congress of Medical Physics (AOCMP) and the 16th South-East Asia Congress of Medical Physics (SEACOMP), Malaysia - International Scholarship from the 74th Japanese Society of Radiological Technology (JSRT), Japan